

TOPICAL REVIEW

## Review on chemical mechanical polishing for atomic surfaces using advanced rare earth abrasives

To cite this article: Xiangyan Chen *et al* 2025 *J. Phys. D: Appl. Phys.* **58** 023004

View the [article online](#) for updates and enhancements.

### You may also like

- [The role of flow field dynamics in enhancing volatile organic compound conversion in a surface dielectric barrier discharge system](#)  
Alexander Böddecker, Maximilian Passmann, Angie Natalia Torres Segura et al.
- [Temperature-dependent properties of wurtzite and rock salt  \$\text{Al}\_{1-x}\text{Sc}\_x\text{N}\$  for applications in BAW resonators](#)  
S Mihalic, E Wade, P Ott et al.
- [Huge photosensitivity gain combined with long photocurrent decay times in various polymorphs of  \$\text{Ga}\_2\text{O}\_3\$ : effects of carrier trapping with deep centers](#)  
A Y Polyakov, E B Yakimov, I V Shchemerov et al.



**UNITED THROUGH SCIENCE & TECHNOLOGY**

**ECS** The Electrochemical Society  
Advancing solid state & electrochemical science & technology

**248th ECS Meeting**  
**Chicago, IL**  
October 12-16, 2025  
*Hilton Chicago*

**Science +  
Technology +  
YOU!**

**SUBMIT ABSTRACTS by March 28, 2025**

**SUBMIT NOW**

A woman with long dark hair, wearing a tan blazer, is smiling and gesturing with her hands. The background features a blue gradient with circular patterns resembling molecular structures.

**Topical Review**

# Review on chemical mechanical polishing for atomic surfaces using advanced rare earth abrasives

Xiangyan Chen<sup>1</sup> , Zhenyu Zhang<sup>1,2,3,\*</sup> , Feng Zhao<sup>1</sup>, Hao Luo<sup>4</sup>, Jianmei Wang<sup>5</sup>, Fanning Meng<sup>2</sup>, Hongxiu Zhou<sup>6</sup>, Xuye Zhuang<sup>7</sup> and Guo Li<sup>8,\*</sup>

<sup>1</sup> State Key Laboratory of High-performance Precision Manufacturing, Dalian University of Technology, Dalian 116024, People's Republic of China

<sup>2</sup> School of Mechanical Engineering, Hangzhou Dianzi University, Hangzhou 310018, People's Republic of China

<sup>3</sup> School of Mechanical and Electrical Engineering, Hainan University, Haikou 570228, People's Republic of China

<sup>4</sup> Baoshan Longi Silicon Materials Co., Ltd, Baoshan 678300, People's Republic of China

<sup>5</sup> School of Mechanical Engineering, Taiyuan University of Science and Technology, Taiyuan 030024, People's Republic of China

<sup>6</sup> School of Energy and Power Engineering, Dalian University of Technology, Dalian 116024, People's Republic of China

<sup>7</sup> School of Mechanical Engineering, Shandong University of Technology, Zibo 255000, People's Republic of China

<sup>8</sup> Research Center of Laser Fusion, China Academy of Engineering Physics, Miyang 621900, People's Republic of China

E-mail: [zzy@dlut.edu.cn](mailto:zzy@dlut.edu.cn) and [liguo51404@163.com](mailto:liguo51404@163.com)

Received 19 March 2024, revised 25 May 2024

Accepted for publication 1 July 2024

Published 23 October 2024

**Abstract**

During the past decades, high-performance devices and setups have been widely used in the fields of precision optics, semiconductors, microelectronics, biomedicine, optoelectronics and aerospace. It is a challenge to achieve ultralow surface roughness free of damages. Due to the unique physicochemical properties of rare earths, ceria has garnered great progresses for atomic surfaces induced by chemical mechanical polishing. Compared with conventional mechanical removal by alumina and silica, rare earth abrasives achieve selective material removal on surface via their special chemical activity, without introducing microscopic scratches and defects. Nevertheless, polishing performance of rare earth abrasives depends on series of factors, e.g. size of abrasive particles, microscale topological structure, configuration of chemical slurry, auxiliary energy fields etc. As a result, it is significant to conduct a comprehensive review to understand state-of-the-art polishing technologies. This review summarizes the effect of polishing slurries composed of different rare earth abrasives on polishing performance under different conditions. Additionally, various energy-assisted

\* Authors to whom any correspondence should be addressed.

polishing strategies are discussed using diverse kinds of rare earth abrasives for distinct polishing forms. Finally, future directions of polishing on rare earth abrasives are addressed.

**Keywords:** rare earth abrasives, chemical mechanical polishing, performance, energy field-assisted polishing, atomic surface

## 1. Introduction

Rare earth elements have been widely applied to metallurgy, petrochemical, optical fiber communication, ultra-precision machining, optoelectronics, microelectronics and aerospace industries, because of their particular physical and chemical properties [1–4]. They can be easily ionized to form trivalent stable ions, in which lanthanum, cerium and europium are the most active [5]. Stable compounds of rare earths form with oxygen, hydrogen, ammonia, sulfur, nitrogen, carbon, and other halogens [6]. Moreover, rare earths can also generate disparate metal compound alloys. Due to these peculiar characteristics, rare earths have been found great applications in chemical mechanical polishing (CMP) [7, 8].

With development of ultra-precision polishing technology [9, 10], demands for ultra-smooth, ultralow-damage surfaces are becoming increasingly apparent. During 1920s, rare earth abrasives were used to polish gun sights of antiaircraft. To date, ultra-precision optics [11], semiconductor processing [12], precision medical care [13], inertial navigation [14] for higher demands on surface quality of high-performance products [15, 16]. Under this background, CMP using rare earth oxide abrasives (mainly CeO<sub>2</sub>) has emerged [17]. Rare earth oxide abrasives exhibit advantages in advanced polishing surface quality, high polishing efficiency, long polishing life, low cost and easy to clean [18, 19], compared to those of traditional abrasives. Nowadays, sizes of ceria varied from  $\mu\text{m}$  to nm have been prepared to meet the industrial and research demands, mainly through solid and liquid phase reaction methods [20].

In the past few decades, rare earth abrasives, such as ceria, have made a profound influence on ultra-precision polishing, and the angstrom surfaces ( $<0.2\text{ nm}$ ) are efficiently achieved [21]. Although the polishing powder has the above excellent performances, it is still unable to meet the processing needs of modern ultra-precision optical components with complex structures. Especially, advanced technologies such as photo-masks and projection lenses in photolithography machines [22–24], fusion and laser weapons lens [25–27], ultra-high quality factor optical microcavity [28–30] all require the use of optical glass with atomic-level surface quality. Consequently, series of work has been conducted to further improve the polishing efficiency and precision. In this regard, diverse polishing technologies are developed, including abrasives, slurries with different components, and energy field assisted polishing technologies [31, 32]. In fact, polishing performance is directly related to topology structure, composite components,

and size of abrasives, as well as slurry composition, specific polishing process and parameters [33]. These works have importantly promoted the development of CMP with rare earth abrasives. Nonetheless, previous researches on CMP using rare earth abrasives have not yet been systematically summarized and discussed.

In this work, recent advancements in CMP are reviewed over the past two decades based on ceria mainly, consisting of development of rare earth abrasives, slurry and advanced composite polishing processes. Meanwhile, the challenges of current research and future directions of CMP with rare earth abrasives are presented. Structure of this review is presented and organized in figure 1. In section 2, the influence of different polishing slurry compositions for macro polishing performance are evaluated, including abrasive types, pH regulators, oxidizer and other additives. In terms of section 3, polishing mechanism of different typical polished materials are explored, mainly contains Si, SiO<sub>2</sub>, SiC, Si<sub>3</sub>N<sub>4</sub> and so on. While in section 4, different energy field assisted polishing devices are discussed and compared. Finally, the section 5 summarizes the current status of rare earth abrasives and provides an outlook on their development prospects in CMP.

## 2. Research on polishing process

### 2.1. Polishing abrasives

In general, the use of abrasives, by means of physical actions such as friction and abrasion, facilitates the elimination of surface irregularities, protrusions, and defects. This process is crucial for the removal of films, oxide layers, or other surface coatings in order to achieve optimal surface planarization [34]. Conventional polishing abrasives, such as Al<sub>2</sub>O<sub>3</sub> and SiO<sub>2</sub>, are typically employed through mechanical friction on the material surface due to their higher hardness compared to rare earth abrasives, aiming to achieve material removal [35]. However, this may result in the introduction of microscopic scratches or surface damage during the polishing process, constraining the formation of the ultimate ultra-precision surface. In contrast, rare earth abrasives utilize unique chemical activity to selectively remove material from the surface, finding widespread application in ultra-precision surface machining. The selection and control of polishing abrasives are paramount to ensuring the desired surface planarity during the CMP process [36, 37]. Different types of abrasives can yield different polishing effects. This chapter primarily focuses on rare earth abrasives used in CMP.

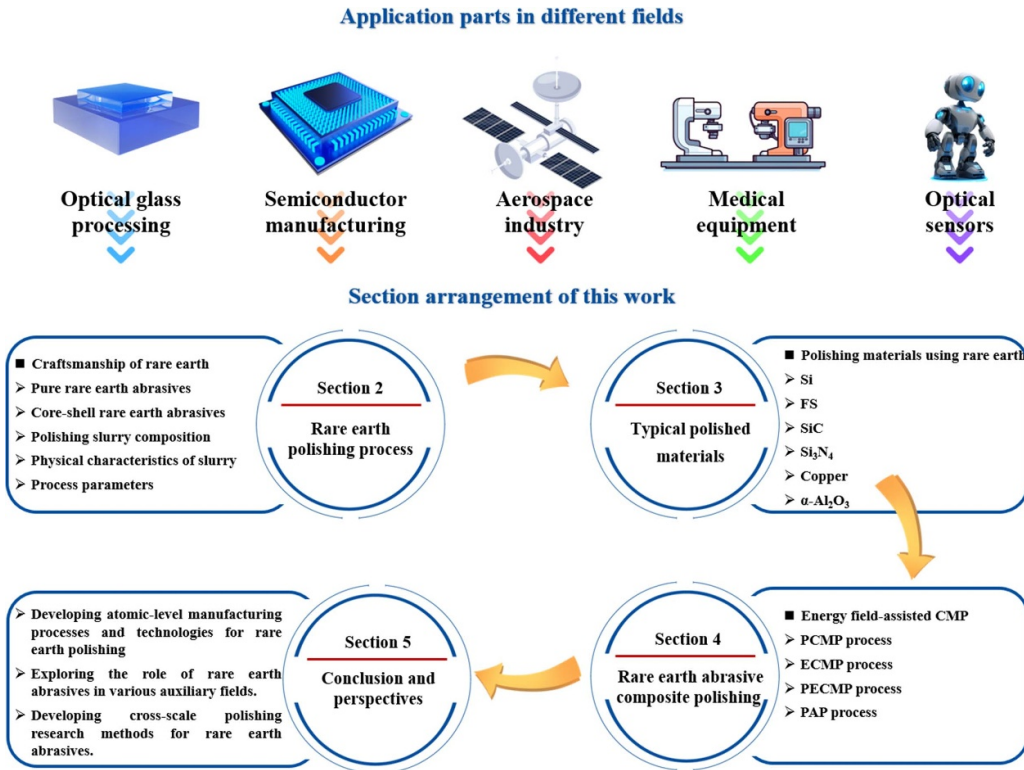


**Figure 1.** Structure of this review paper and the application of rare earth abrasives in various areas.

**2.1.1. Pure rare earth abrasives.** Pure rare earth abrasives mainly refer to pure rare earth abrasives and pure rare earth abrasives doped with other elements, typically obtained through processes such as smelting, chemical synthesis, or purification. In CMP, chemically synthesized methods, such as the precipitation method [38], sol–gel method [39], homogenous precipitation [40], urea condensation [41], co-precipitation method, and hydrothermal synthesis are commonly selected for pure rare earth abrasives. The scanning electron microscopy (SEM) images in figure 2 illustrate the morphological characteristics of the novel pure rare earth abrasives. It can be observed that rare earth abrasives come in various shapes, including circular, polygonal, rod-like forms etc. The nanoclustered and highly crystalline cerium oxide nanoparticles (NPs), as shown in figures 2(a) and (b), presenting circular and polygonal shapes. Studies indicate that nanoclustered NPs in circular shape exhibit low crystallinity and a high Ce<sup>3+</sup>/Ce<sup>4+</sup> ratio [42]. Ho *et al* developed a new spindle-like CeO<sub>2</sub> in figure 2(c), the band gap energy of the sample was determined by Ultraviolet–Vis spectroscopy as rod-shaped > spherical > spindle-like [43]. The particles prepared from different cerium precursors are shown in figures 2(d)–(g), and the comparison reveals that particles prepared from oxides exhibit better uniformity in cerium oxide particle distribution [44]. The CeO<sub>2</sub> NPs (figure 2(h)) synthesized with urea condensation by Wang *et al* exhibit excellent monodispersity [41]. Lim *et al* studied the influence of CeO<sub>2</sub> abrasive particle (figure 2(i)) size on the height of oxide steps and the amount of dishing [45]. In general, different shapes of CeO<sub>2</sub> abrasive are suitable for various machining needs

and workpiece characteristics. Rod-shaped abrasives typically have sharper edges, providing a certain directional effect during machining, aiding in controlling the grinding path and direction, allowing for finer grinding in local areas. Polygonal abrasives have multiple grinding surfaces, enabling simultaneous grinding in different directions, better adapting to the curvature and angles of the workpiece surface, improving machining efficiency. Flat abrasives are particularly advantageous for machining flat surfaces due to their enhanced controllability, which minimizes errors and enhances machining precision. Spherical abrasives with smooth surfaces and no sharp edges tend to produce fewer scratches and obtain higher surface quality on material surface, and it is possible to obtain atomic surface [46].

Moreover, the effectiveness of ceria abrasives can be boosted by doping elements like Y, La and Zr. Ultra-smooth surface can be obtained after polishing with appropriate CeO<sub>2</sub> abrasive [47]. The surface roughness Ra (within  $5 \times 5 \mu\text{m}^2$ ) and material removal rate (MRR) of SiO<sub>2</sub> after polishing with CeO<sub>2</sub>, porous ceria (pCeO<sub>2</sub>), Zr-doped pCeO<sub>2</sub> (pCeZrO<sub>2</sub>), Gd-doped pCeO<sub>2</sub> (pCeGdO<sub>2</sub>) [48], CeO<sub>2</sub>-Air, CeO<sub>2</sub>-Ar, CeO<sub>2</sub>-Ar/H<sub>2</sub> [49], Ce<sub>0.9</sub>La<sub>0.1</sub>O<sub>2</sub>, Ce<sub>0.8</sub>La<sub>0.2</sub>O<sub>2</sub>, Ce<sub>0.7</sub>La<sub>0.3</sub>O<sub>2</sub> [50], Ce<sub>0.96</sub>Y<sub>0.02</sub>Pr<sub>0.02</sub>O<sub>2</sub> [19] abrasives are shown in figure 3. It can be observed that using porous ceria for polishing SiO<sub>2</sub> yields a smoother surface. Ceria doped with La exhibits the highest Ra and MRR. Moreover, ceria synthesized in a reducing gas environment demonstrates superior polishing performance compared to ceria synthesized in air.

Abrasive size is another factor that have huge impact on the polished surface roughness. Among them, using smaller

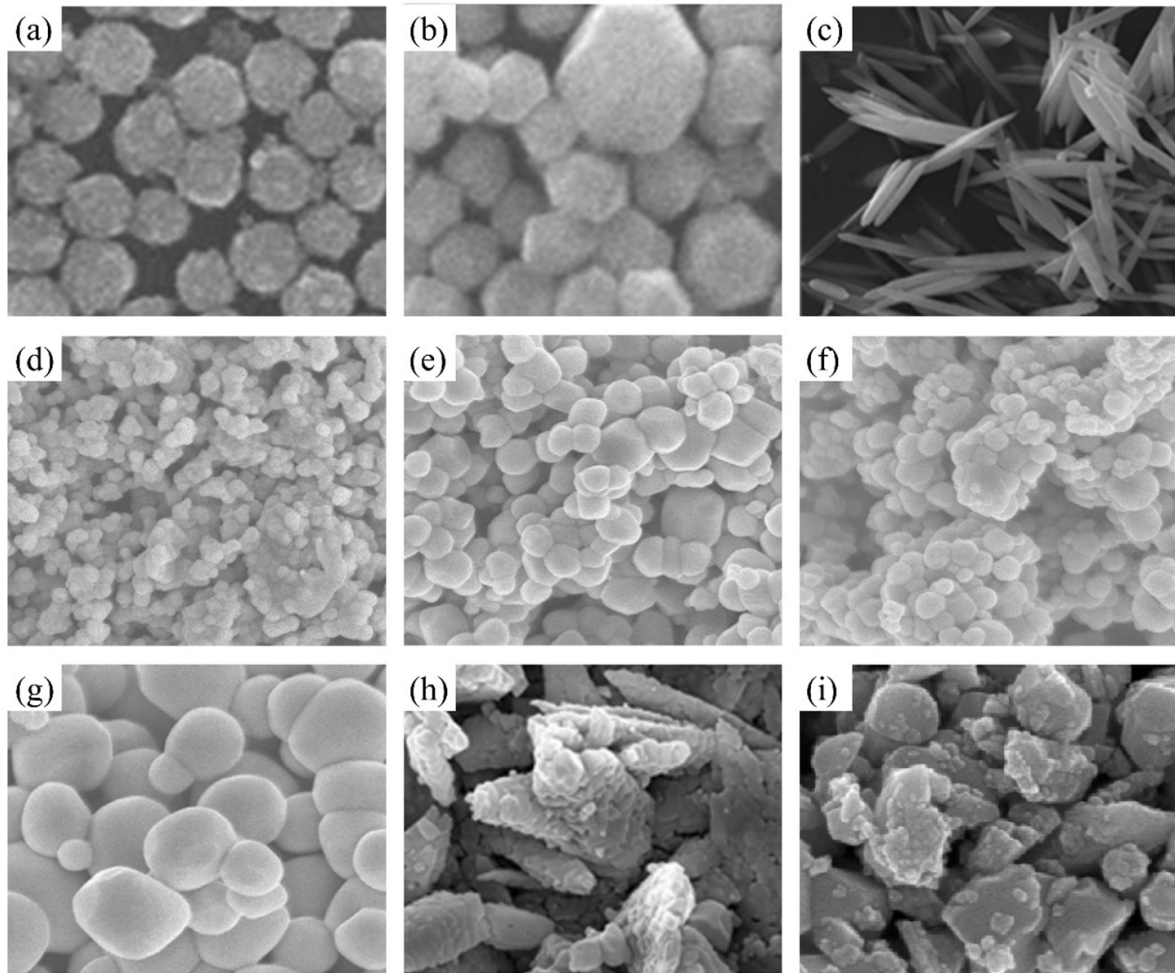


**Figure 2.** SEM images of pure rare earth abrasives with different structures: (a) Nanoclustered ceria abrasive. (b) Highly crystalline ceria abrasive. (c) Spindle-like CeO<sub>2</sub> abrasive. (d) Ce(OH)<sub>4</sub> abrasive. (e) CeN abrasive. (f) CeCl<sub>3</sub> abrasive. (g) Irregular elliptical-shape CeO<sub>2</sub> abrasive. (h) A strip CeO<sub>2</sub> abrasive combination. (i) Polygonal-shaped CeO<sub>2</sub> abrasive. (a), (b) Reproduced from [42], with permission from Springer Nature. (c) Reprinted with permission from [43]. Copyright (2005) American Chemical Society. (d)–(g) Reprinted from [44], Copyright (2011), with permission from Elsevier. (h) Reproduced from [41], with permission from Springer Nature. (i) Reprinted from [45], Copyright (2005), with permission from Elsevier.

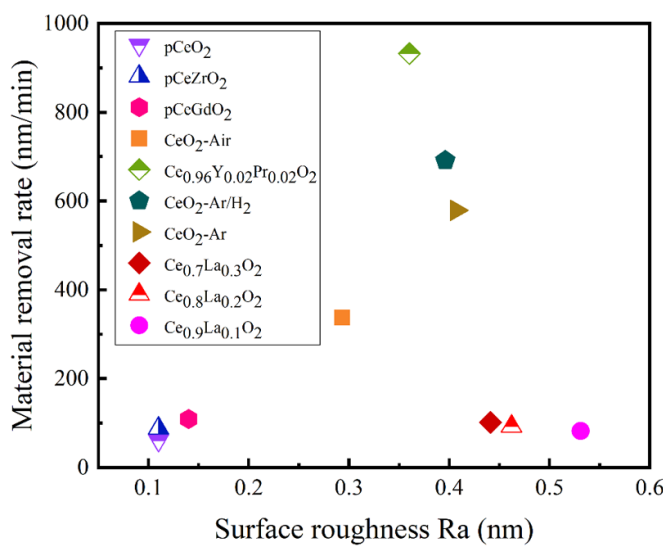


**Figure 3.** Material removal rate-surface roughness data of different types of pure rare earth abrasives.

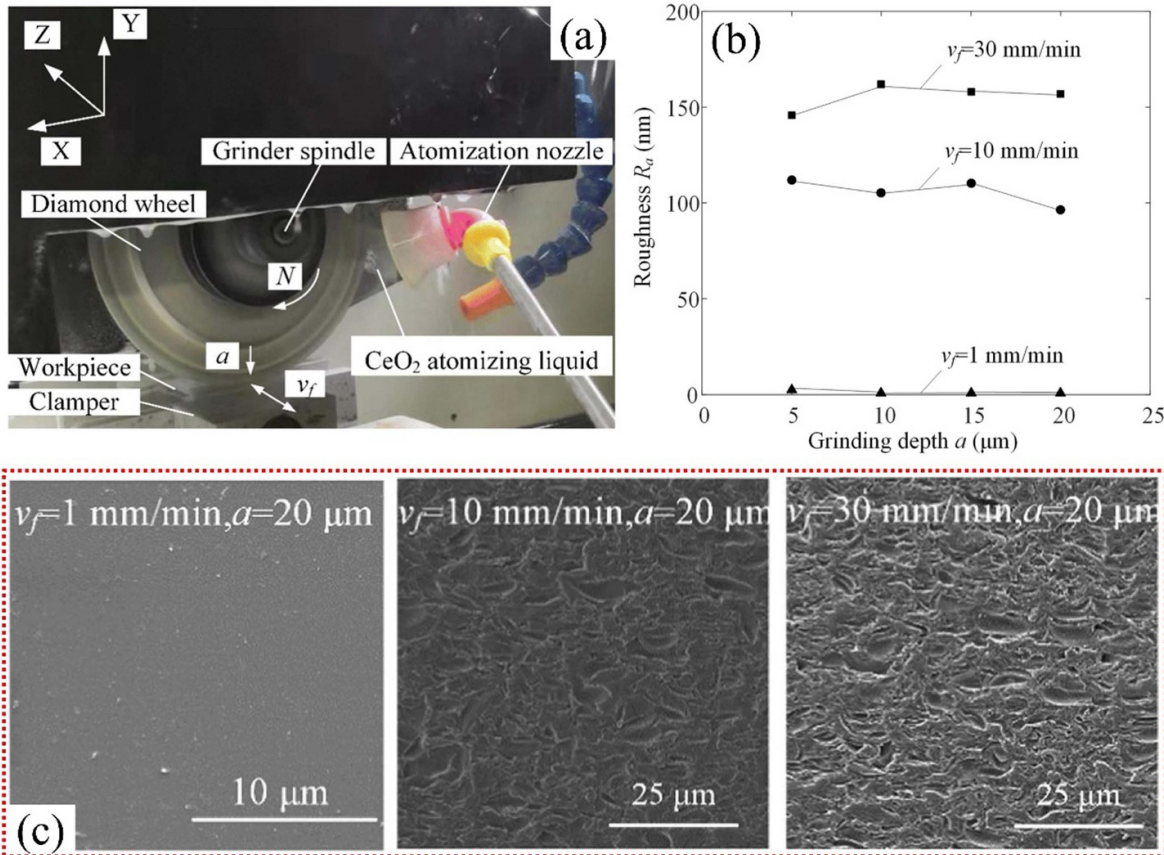


**Figure 4.** (a) The experimental scene schematic of axis-feed grinding. (b) Surface roughness obtained at different feed rates and grinding depths. (c) Surface morphology obtained at different feed rates and grinding depths. (a)–(c) Reproduced from [56], with permission from Springer Nature.

abrasives tends to result in a higher edge removal rate compared to using larger abrasives [51, 52]. Therefore, during the polishing process, larger-sized abrasives can be initially used to achieve a certain surface precision in the shortest possible time, and then smaller-sized abrasives can be employed to polish the material surface to achieve a level of smoothness close to atomic-level cleanliness [53].

Essentially, rare earth abrasives exist not only in powder form but also in a gel (hydrosol) state [54, 55]. Nano cerium dioxide sol can be synthesized through the sol-gel process. Kim *et al* utilized two colloidal ceria abrasives, NC-ceria and CF-ceria, for polishing SiO<sub>2</sub> [42]. Verified through experimental analysis, nanocluster ceria abrasives possess both physical pliancy and chemical reactivity, exhibiting outstanding SiO<sub>2</sub> removal capability. The MRR is 890.4 nm min<sup>-1</sup>, showing significant potential for scratch inhibition in CMP processing.

Noticed that the pure ceria abrasives are already capable for generating atomic surface roughness. The core mechanism for doping different elements in the ceria abrasives is to increase the concentration of Ce<sup>3+</sup>. As a result, the oxygen vacancy in the abrasives increases which can greatly promote the MRR. Another breakthrough of application would be the addition of ceria into the grinding fluid, which cleverly introduces the polishing mechanism into grinding of hard brittle materials

to obtain better surface roughness and lower surface damage. Zhang *et al* introduced a novel axis-feed grinding approach, assisted by pure CeO<sub>2</sub> atomizing liquid [56]. The experimental scene in figure 4(a). This approach employed relatively large-grain diamond grinding wheels and substantial grinding depth to achieve a nearly polished surface roughness. Ultimately, as shown in figures 4(b) and (c), at a feed rate of 1 mm min<sup>-1</sup> and a grinding depth of 20  $\mu\text{m}$ , the optimal roughness was 1.05 nm, which was originally believed not possible for grinding on such low precision grinding machine using pure water for cooling. The near polished surface roughness is a solid proof for the effectiveness of ceria abrasives in lowering fracture rate and promote surface quality.

**2.1.2. Core-shell rare earth abrasives.** For decades, composite abrasives have been widely used in CMP. Among the various types of abrasives available, CeO<sub>2</sub>-based NPs have gained significant popularity and are extensively employed in traditional CMP applications. These NPs are particularly effective in removing silica materials due to their well-established chemical-tooth action. Several cost-effective methods for synthesizing core-shell abrasives, including ceria are solvo-thermal approach, sol-gel technique, self-assembly process, electrochemical synthesis, and micro-emulsion

**Table 1.** Core–shell rare earth abrasives summary.

Abrasives	Polished material	Ra (nm)	MRR (nm/min)	Measuring range ( $\mu\text{m} \times \mu\text{m}$ )	References
PS/PANI/CeO <sub>2</sub>	SiO <sub>2</sub>	0.122	81		[64]
PMMA/CeO <sub>2</sub>	SiO <sub>2</sub>	0.154	266.2		[65]
mSiO <sub>2</sub> @CdS@CeO <sub>2</sub>	SiO <sub>2</sub>	0.134	NA		[66]
mSiO <sub>2</sub> @CeGdO <sub>2</sub>	SiO <sub>2</sub>	0.137	NA		[67]
Cs/CeO <sub>2</sub>	SiO <sub>2</sub>	0.11	93–127		[68]
Cs/CeYO <sub>2</sub>		0.10	128–150		[68]
mSiO <sub>2</sub> /CeO <sub>2</sub>	SiO <sub>2</sub>	NA	38–66		[69]
mSiO <sub>2</sub> /Ce <sub>0.83</sub> Er <sub>0.17</sub> O <sub>2</sub>		NA	71–99		
PS/CeO <sub>2</sub>	SiO <sub>2</sub>	0.11	26	5 × 5	[70]
D-mSiO <sub>2</sub> /CeO <sub>2</sub>		0.15	85		
Ce <sub>0.92</sub> La <sub>0.08</sub> O <sub>2</sub>	SiO <sub>2</sub>	0.648	562.66		[71]
Ce <sub>0.92</sub> Pr <sub>0.08</sub> O <sub>2</sub>		0.628	578.74		
Ce <sub>0.92</sub> Y <sub>0.08</sub> O <sub>2</sub>		0.509	626.97		
SiO <sub>2</sub> /CeO <sub>2</sub>	Si-Face 6 H-SiC	0.216	20.12		[72]
PS@CeO <sub>2</sub> :La	UTG	0.32	480.22		[73]
PS@CeO <sub>2</sub> /DND	Sapphire wafer	0.52	23.33–28.33		[74]
Polyurethane-CeO <sub>2</sub>	SiC	0.51	50–66.67	720 × 540	[75]
CeO <sub>2</sub> –TiO <sub>2</sub>	RB-SiC	1.112	9.817		[32]
PS/CeO <sub>2</sub>		0.589	14.633	2.5 × 2.5	
PS/CeO <sub>2</sub> –TiO <sub>2</sub>		0.497	20.383		

NA (Not available).

PS/PANI/CeO<sub>2</sub> (Polystyrene/Polyaniline/Ceria).

PMMA/CeO<sub>2</sub> (Polymethylmethacrylate/Ceria).

method [57]. There are also some polishing abrasives specifically designed for magnetic field-assisted polishing, with a removal rate significantly higher than traditional abrasives.

It is widely recognized that the polishing characteristics of CeO<sub>2</sub> abrasives are greatly influenced by factors such as size, shape, structure, component composition, and surface defects (Vo and Ce<sup>3+</sup>) at the nanoscale. To date, various types of CeO<sub>2</sub>-involved abrasives including core–shell structured [58], porous [42], metal-doped [59], non-spherical [60, 61], hybrid or mixed [62, 63]. Multiple novel polishing abrasives have been synthesized to enhance material surface quality and removal efficiency in CMP practice. A summary of Ra and MRR data obtained using core–shell rare earth abrasives on different materials can be found in table 1.

Numerous investigations have already been conducted on the synthesis and polishing effects of rare earth composite abrasives. The shape and function of abrasives synthesized through different methods vary, leading to differing effects on material surface quality and removal. Figure 5 illustrates the morphology of several different rare earth abrasives, and it can be observed that their shapes are varied. A three-step strategy is employed to construct hybrids of mSiO<sub>2</sub>@CdS@CeO<sub>2</sub> abrasives in figure 5(a), featuring mesoporous cores and double-layered core–shell heterostructures. The formation of the CdS-CeO<sub>2</sub> heterojunction facilitates efficient separation of photogenerated charge carriers and high activity oxygen production, bolstering the formation of photochemically reacted layers [66]. The core–shell structured PS@CeO<sub>2</sub>:La abrasives as shown in figure 5(b), the discovery indicates that La<sup>3+</sup> has a more pronounced modulation effect on lattice distortion and Ce<sup>3+</sup>/Ce<sup>4+</sup> chemical shift [73]. Figure 5(c) depicts CS/CeYO<sub>2</sub> core–shell abrasives, which

effectively enhance the removal rate [68]. The ternary composite abrasive PS@CeO<sub>2</sub>/DND (figure 5(d)) increases the polishing interface area under the joint action of the three components [74]. Under the influence of a strong electric field between electrodes, polyurethane (PU)-CeO<sub>2</sub>) core–shell abrasives (figure 5(e)) exhibit durability [75]. Compared to figure 5(f), the abrasive shown in figure 5(h) adheres CeO<sub>2</sub> and Fe<sub>3</sub>O<sub>4</sub> abrasives unevenly to the polymer abrasives at a lower temperature of about 80 °C. Under the action of a magnetic field, the removal rate of this abrasive is significantly higher than that of conventional abrasives [76]. Chen *et al* developed various composite abrasives, PMMA/CeO<sub>2</sub> hybrid abrasives (figure 5(g)) can be used to produce polishing pads [65], mSiO<sub>2</sub>@CeGdO<sub>2</sub> (figure 5(i)) abrasives can significantly enhance the removal efficiency under ultraviolet light irradiation [67].

The monodispersity and morphology of abrasives are recognized as crucial factors influencing polishing rates [77–80]. The size and morphology of ceria abrasives can be regulated through the structure of ceria-coated silica nanoparticles [81]. It has been demonstrated that the slurry prepared using these nano-particles can enhance the selectivity between SiO<sub>2</sub> and SiN, thus increasing the selective removal rate [82]. Nevertheless, achieving monodispersity and morphology control for larger ceria abrasives remains a challenge due to the difficulty in controlling the particle growth of ceria [83].

The investigation revealed that the surface of CeO<sub>2</sub> abrasives throughout the polishing process contains not only Ce<sup>4+</sup> but also a certain amount of Ce<sup>3+</sup> [84]. Doping trivalent ions generates a significant number of oxygen vacancies [85], which promotes the formation of Ce<sup>3+</sup> on the CeO<sub>2</sub> crystal

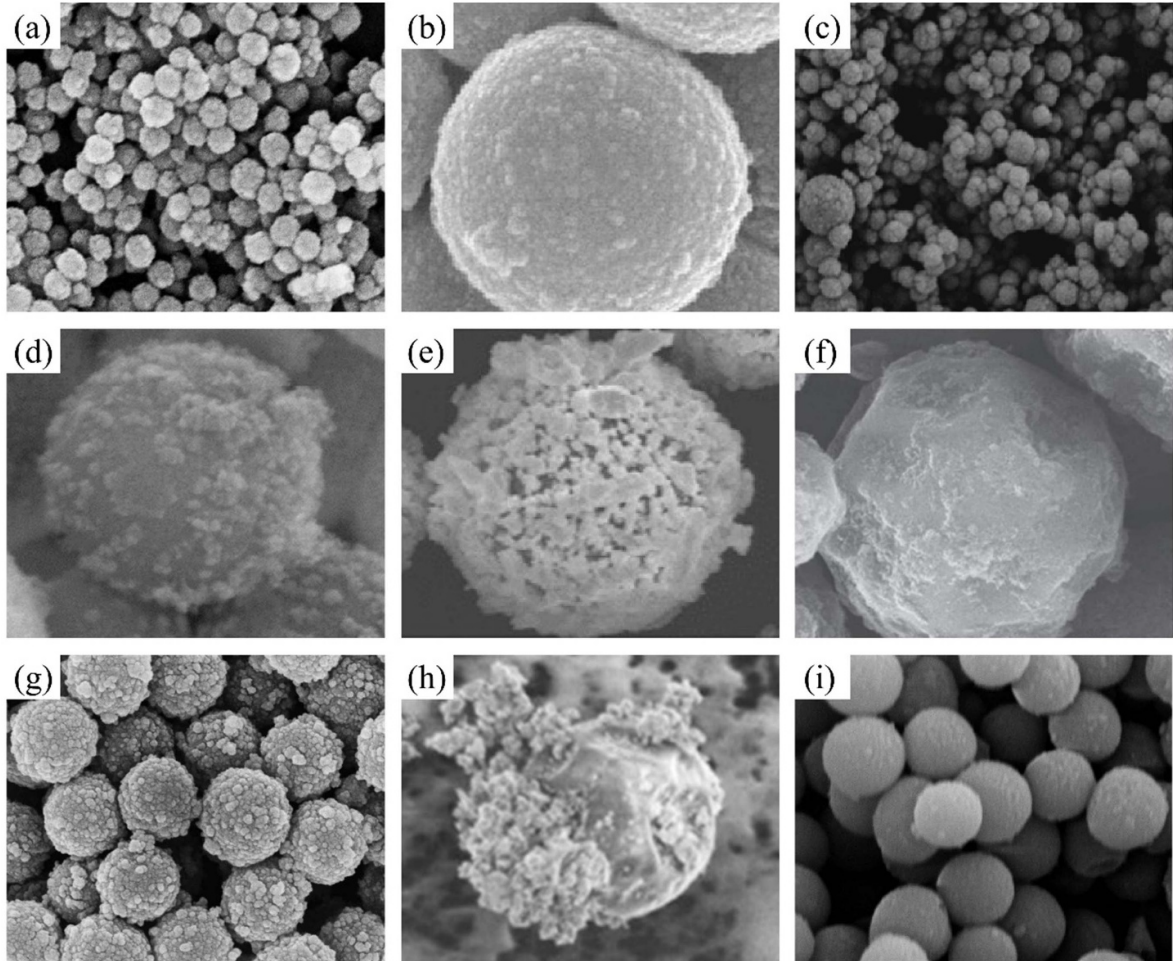


**Figure 5.** SEM images of composite rare earth abrasives. (a)  $\text{mSiO}_2@\text{CdS}@Ce\text{O}_2$  abrasive. (b)  $\text{PS}@Ce\text{O}_2:\text{La}$  abrasive. (c)  $\text{CS}/Ce\text{YO}_2$  abrasive. (d)  $\text{PS}@Ce\text{O}_2/\text{DND}$  abrasive. (e)  $\text{PU}-Ce\text{O}_2$  abrasive. (f)  $\text{Polymer}/Ce\text{O}_2-\text{Fe}_3\text{O}_4$  abrasive. (g)  $\text{PMMA}/Ce\text{O}_2$  hybrid abrasive. (h)  $\text{Polymer}/Ce\text{O}_2-\text{Fe}_3\text{O}_4$  abrasive. (i)  $\text{mSiO}_2@Ce\text{GdO}_2$  abrasive. (a): Reprinted from [66], Copyright (2023), with permission from Elsevier. (b): Reprinted from [73], Copyright (2023), with permission from Elsevier. (c): Reprinted from [68], Copyright (2022), with permission from Elsevier. (d): Reprinted from [74], Copyright (2021), with permission from Elsevier. (e): Reprinted from [75], Copyright (2017), with permission from Elsevier. (f) and (h): Reprinted from [76], Copyright (2016), with permission from Elsevier. (g): Reprinted from [65], Copyright (2015), with permission from Elsevier. (i): Reprinted from [67], Copyright (2023), with permission from Elsevier.

compared to other ions [86]. The bonding strength between ceria and  $\text{SiO}_2$ , along with the rate of ceria NPs attachment onto a  $\text{SiO}_2$  surface, exhibited an upward trend in correlation with the surface concentration of  $\text{Ce}^{3+}$ , improving polishing precision and achieving surfaces with precision and ultra-precision machining [87, 88]. Generally, experimental validation has confirmed that doping with  $\text{Ce}^{3+}$  enhances CMP performance of  $\text{CeO}_2$  abrasives, leading to modifications in their properties. However, additional research is necessary to gain a deeper comprehension of how various doping types and quantities affect the crystal structure, microscopic morphology, and presence of defects in  $\text{CeO}_2$  abrasives. Studies have demonstrated that doping with  $\text{Y}^{3+}$ ,  $\text{La}^{3+}$ , and  $\text{Pr}^{3+}$  can significantly increase the concentration of  $\text{Ce}^{3+}$  on the surface of  $\text{CeO}_2$  abrasives [50].  $\text{Y}^{3+}$  doping is more favorable for the transition from  $\text{Ce}^{4+}$  to  $\text{Ce}^{3+}$  compared to  $\text{La}^{3+}$  and  $\text{Pr}^{3+}$  doping [71]. The introduction of dopants (La, Nd, and Yb) can promote the formation of oxygen vacancies in  $\text{CeO}_2$  and the transformation of  $\text{Ce}^{4+}$  to  $\text{Ce}^{3+}$  [89]. Abrasives

with zeta potential dependency notably enhance MRR [90]. Yuan *et al* synthesized composite abrasives called  $\text{CeO}_2@ZIF-8$  [91]. The incorporation of ZIF-8 onto the surface of  $\text{CeO}_2$  promotes the creation of additional oxygen vacancies within the cerium lattice, as depicted in figure 6(a). Consequently, an increased number of  $\text{Ce}^{3+}$  ions become exposed on the surface of  $\text{CeO}_2@ZIF-8$  abrasives [92], leading to enhanced polishing performance. The principle of CMP on glass surface is illustrated in figure 6(b).

Based on above section, it can be seen that the lowest surface roughness is achieved by pure rare earth abrasives. The main purpose of fabricating composite rare earth abrasives is to achieve higher MRR utilizing the special mechanism between additives and the ceria. Doping of elements like Y, La, Pr and Nd are also frequently found on core–shell rare earth abrasives, which also serves the same purpose of increasing oxygen vacancy. Different mechanical or chemical properties of the core and the shell material are successfully coupled to combine the advantage of both materials. But the cost and the

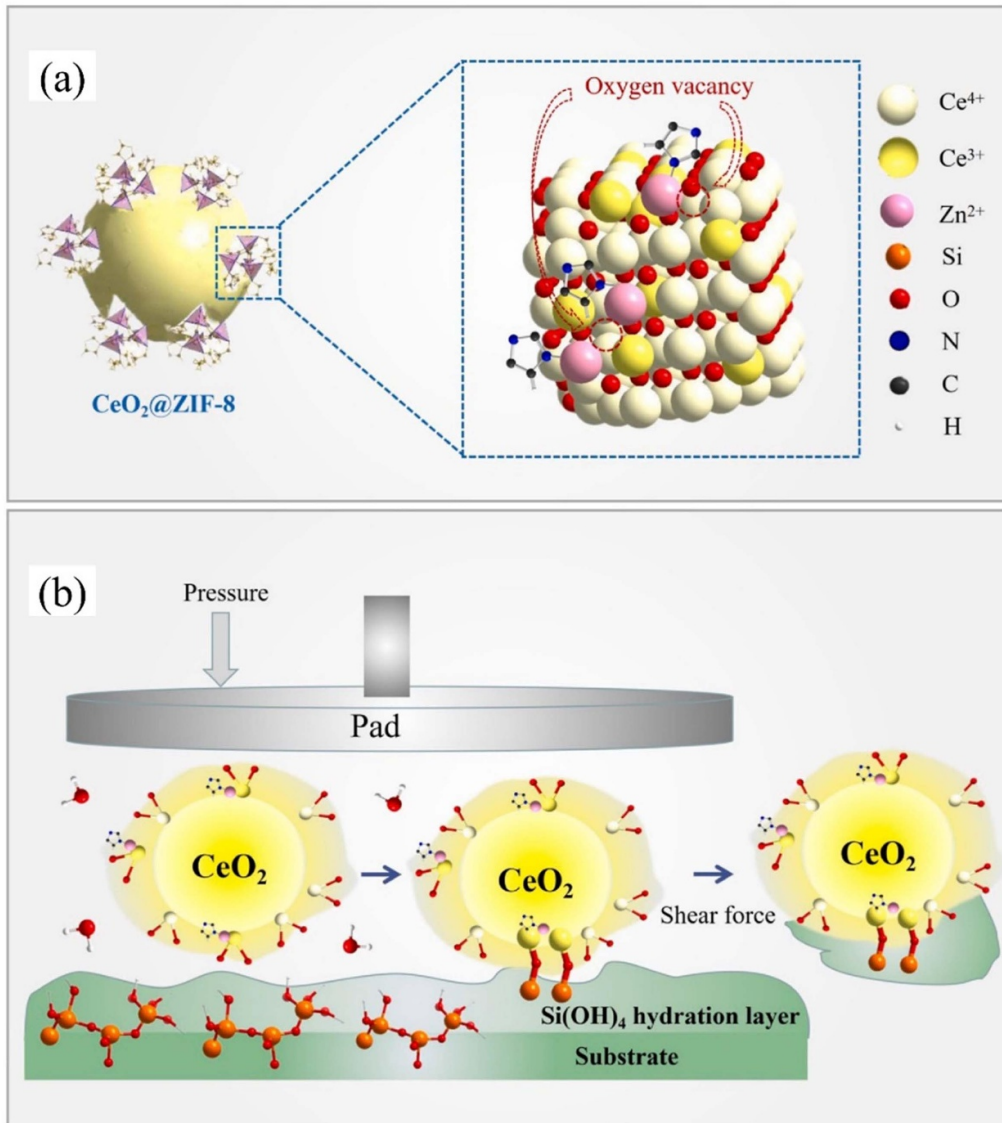


**Figure 6.** (a) The space filling model of the  $\text{CeO}_2@\text{ZIF-8}$  surface structure. (b) Principle of polishing glass using  $\text{CeO}_2@\text{ZIF-8}$  abrasive. (a) and (b): Reprinted from [91], Copyright (2023), with permission from Elsevier.

fabrication complexity continue to hinder the grant application of core–shell abrasives in manufacturing. In the future, it would continuously be a hot topic for new fabrication and doping techniques.

## 2.2. Polishing slurry composition

In general, a polishing slurry consists of abrasives, the base solution, pH adjusters, dispersants, oxidizing agents, and other components [93, 94]. Each component serves distinct functions to ensure the slurry's excellent performance [95]. However, the majority of polishing slurries mentioned in the literature often consist of more than four components and involve the utilization of potent acids, alkalis, or hazardous chemicals. These slurries not only have the potential to corrode polishing equipment but also pose significant risks to both the

environment and operators. Furthermore, effectively removing any remaining surface attachments following the CMP process presents a formidable challenge [96, 97]. In contrast, the utilization of polishing slurries prepared with rare earth abrasives does not cause environmental pollution, achieving the effect of environmentally friendly and green polishing [21]. The summary of surface roughness and MRR values after polishing with different polishing slurries on different materials is listed in table 2.

**2.2.1. The dispersant.** In the polishing process, there are situations where it is inconvenient to use physical stirring for the polishing slurry. This leads to precipitation, aggregation, and stratification of the polishing slurry, causing variations in the composition of the polishing slurry used during the

**Table 2.** Typical rare earth abrasive polishing slurries composition.

Abrasives	Composition of polishing slurry	Polished material	Ra /Sa (nm)	MRR (nm/min)	Measuring range ( $\mu\text{m} \times \mu\text{m}$ )	References
CeO <sub>2</sub>	Na <sub>2</sub> CO <sub>3</sub> and DIW	SiO <sub>2</sub>	Sa = 0.093	125.34	20 × 20	[98]
CeO <sub>2</sub>	h-BN nanoflakes, KOL, and DIW	SiO <sub>2</sub>	Sa = 0.124	532	10 × 10	[99]
CeO <sub>2</sub>	LaOF, K <sub>4</sub> P <sub>2</sub> O <sub>7</sub> , SNLS, PAAS and DIW	SiO <sub>2</sub>	Sa = 0.23	530.52	50 × 50	[100]
CeO <sub>2</sub>	SA, SDS and DIW	SiO <sub>2</sub>	Sa = 0.08	553.58	20 × 20	[21]
Colloidal ceria	KMnO <sub>4</sub> at pH 2	6 H-SiC	Ra = 0.11	18.15	2 × 2	[101]
CeO <sub>2</sub>	(NaPO <sub>3</sub> ) <sub>6</sub> , CH <sub>3</sub> COOH	P-Si (100)	NA	412	NA	[102]
CeO <sub>2</sub>	DIW, acrylic	STI	NA	288.3	NA	[103]
CeO <sub>2</sub>	Corn oil, Na <sub>2</sub> CO <sub>3</sub> solution, and polysorbate	KDP	Sa = 0.648	644	100 × 100	[104]
CeO <sub>2</sub>	SiO <sub>2</sub> , H <sub>2</sub> O <sub>2</sub> , NaHCO <sub>3</sub> , Polyaspartic acid and DIW	Cu	Sa = 0.092	NA	50 × 50	[105]
SiO <sub>2</sub> /CeO <sub>2</sub>	H <sub>2</sub> O <sub>2</sub> , GLY, BTA, NaOH	Cu	Ra = 0.363	279	5 × 5	[106]
CeO <sub>2</sub>	H <sub>2</sub> O, dilute hydrochloric acid	Lime glass	Sa = 1.56	365.5	500 × 500	[107]
CeO <sub>2</sub> –NH <sub>2</sub>			Sa = 1.53	370.33		
CeO <sub>2</sub> –EDTA			Sa = 1.31	490.5		

NA (Not available).

polishing process, thus failing to achieve the desired polishing effect. Therefore, it is necessary to add dispersant to the polishing slurry to maintain the dispersion of abrasives, prevent their agglomeration, ensure uniform distribution on the surface during polishing, and enhance the stability of the polishing slurry to prevent component stratification or precipitation, maintaining consistent polishing results.

Anionic dispersants help prevent the aggregation and accumulation of abrasives, maintaining the uniform dispersion of abrasives in the polishing slurry. In order to maintain the stability of polishing slurries, two types of anionic dispersants are commonly used, sodium N-lauroyl sarcosinate (SNLS) and sodium polyacrylate (PAAS). These dispersants ensure that the abrasives in the slurry have a more uniform particle size distribution, resulting in a smoother surface after polishing [100]. Additionally, organic acids such as acetic acid, propionic acid, lactic acid, and citric acid are frequently employed as dispersants in CMP [108]. The evaluation of dispersion stability reveals that using acetic acid with CeO<sub>2</sub> suspension leads to moderate particle size distribution, good stability (zeta potential >50 mV), monodispersity (polydispersity index <0.1), and higher chemical activity due to increased Ce<sup>3+</sup> content [109]. This ultimately results in a higher removal rate.

Various polymers with different functional groups can be introduced as non-ionic surfactants during the preparation process of CeO<sub>2</sub> slurry, including polyethylene glycol (PEG), polyacrylamide, polyvinylpyrrolidone (PVP-K30), polyvinyl alcohol (PVA-124), and polypropylene glycol [110]. The experiment indicates that elevated zeta potential values can improve particle dispersion when using deionized water-based slurries [111], and non-ionic surfactants with more C–O bonds exhibit stronger dispersing effects and greater adsorption

capacity on Si<sub>3</sub>N<sub>4</sub> surfaces. Therefore, selecting the appropriate dispersant is of crucial significance for enhancing the polishing effectiveness.

**2.2.2. pH regulators.** To comprehend the ceria-silica CMP mechanisms, certain researchers conducted an investigation on the influence of cerium slurry pH on the removal efficiency and surface morphology of silicon dioxide [112]. When adjusting the pH values using HCl and KOH, low removal rates of silica were observed in highly acidic conditions, with the maximum removal efficiency occurring when the pH reached 6.0 [113]. In conditions with pH ranging from neutral to alkaline, moderate rates of silica removal were observed. The acceleration in the removal rate beyond pH 9 can be attributed to an enhanced dissolution of silica. It is evident that the efficiency of ceria slurries in removing silica is greatly influenced by pH, reaching its maximum near the isoelectric point of the ceria slurry.

The electrostatic interactions between the abrasives and the wafer surface is significantly influenced by their individual zeta potentials [41]. When abrasives and wafer surfaces carry opposite charges, electrostatic attraction accelerates the polishing rate of the wafer material. Figure 7 compares the zeta potentials of pristine CeO<sub>2</sub> NPs and silicon dioxide surfaces [89]. When the pH of the slurry exceeds 6.5 or falls below 3.2, electrostatic repulsion occurs, resulting in a slower polishing rate. Conversely, when the pH of the slurry is within the range of 3.2–6.5, electrostatic attraction occurs, leading to an accelerated polishing rate. This explains why the MRR of SiO<sub>2</sub> is higher in acidic slurries than in alkaline slurries.

Several studies have been conducted to investigate the impact of different non-ionic surfactants in CeO<sub>2</sub>-based slurries at varying pH values on MRR, selectivity of removal, and surface quality during wafer polishing. The experimental

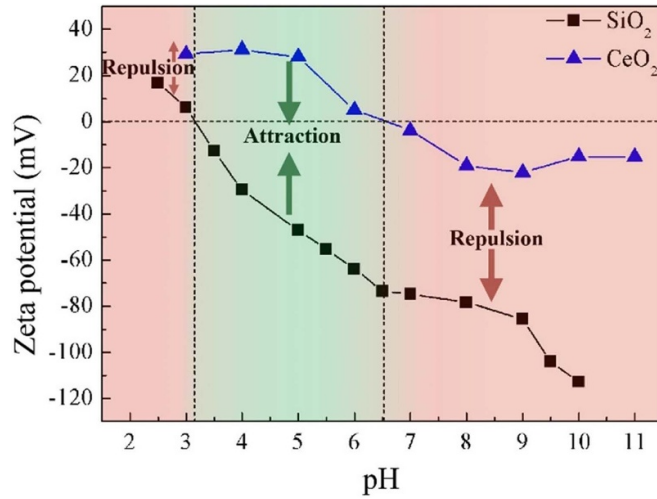


**Figure 7.** Zeta potential curve of pristine  $\text{CeO}_2$  nanoparticles and silica surface changed with slurry pH. Reprinted from [89], Copyright (2020), with permission from Elsevier.

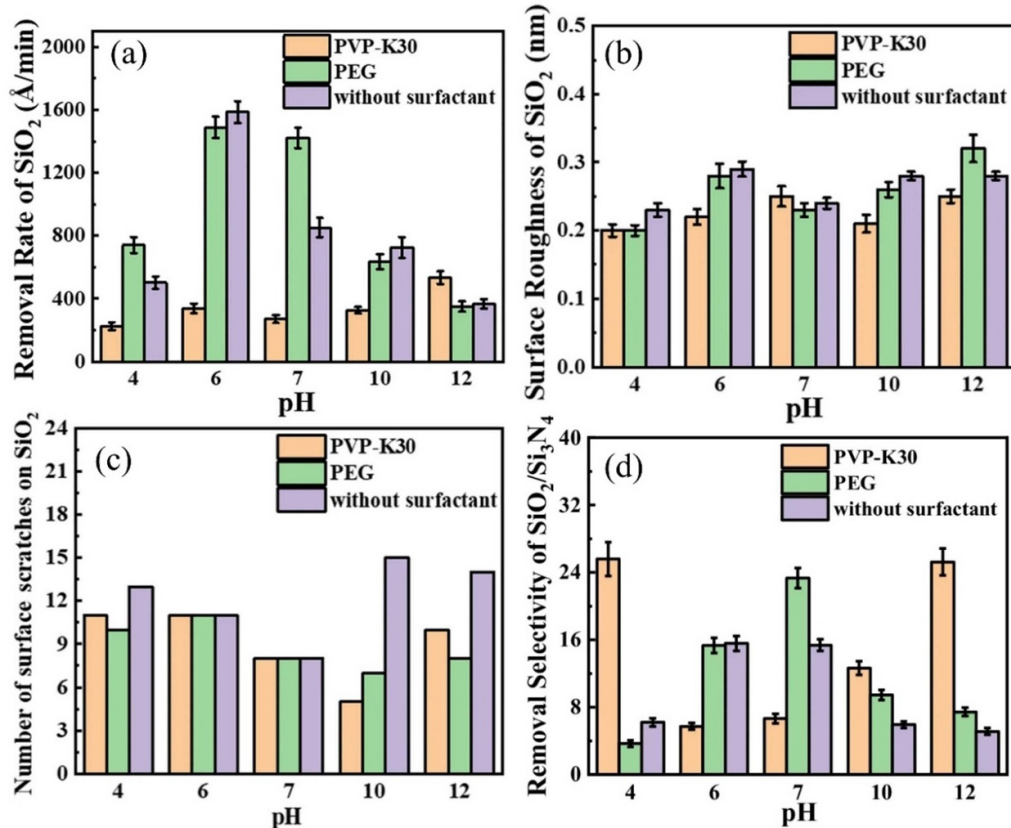


**Figure 8.** (a) Removal rate, (b) surface roughness, (c) surface scratches count of  $\text{SiO}_2$ , and (d) removal selectivity between  $\text{SiO}_2$  and  $\text{Si}_3\text{N}_4$  after  $\text{CeO}_2$  slurries polished with/without PVP-K30 and PEG at different pH values. (a)–(d): Reprinted from [110], Copyright (2023), with permission from Elsevier.

results demonstrate that at pH values of 4, 6, 7, and 10, non-ionic surfactant polyethylpyrrolidone (PVP-K30) exhibits a stronger inhibitory effect on  $\text{SiO}_2$  MRR compared to PEG (figure 8(a)) [110]. The reason for this is due to the smaller zeta potential of the PVP-K30 mixed suspension with  $\text{CeO}_2$  compared to that of the PEG mixed suspension, resulting in a more

powerful repulsion between the suspension and  $\text{SiO}_2$ . PVP-K30 demonstrates selective removal properties in both acidic and alkaline environments, while PEG shows significant removal effectiveness in neutral pH environments (figure 8(b)). The surface roughness of  $\text{SiO}_2$  polished with  $\text{CeO}_2$  slurries containing either PVP-K30 or PEG remains between 0.20 nm and

0.32 nm (figure 8(c)). Moreover, the addition of PVP-K30 and PEG reduces the number of scratches on the polished  $\text{SiO}_2$  surface, with fewer scratches observed in alkaline environments compared to acidic ones (figure 8(d)).

**2.2.3. The oxidizer.** In the polishing slurry, the incorporation of an oxidizing agent serves to oxidize the material layer, generating a pliable and active oxide film on the surface, aiding in material removal. The corrosion rate is significantly influenced by the type and concentration of the oxidant. When the oxidation potential or concentration is low, the fraction of the reacted surface is low, leading to hard contact between the abrasives and the surface and more surface defects. Conversely, a compact and rigid oxide layer may develop, impeding subsequent mechanical removal. Hence, varying oxidizer types or adjusting concentrations is imperative for different materials [114]. The commonly used oxidizer primarily include hydrogen peroxide ( $\text{H}_2\text{O}_2$ ) [115], ozone ( $\text{O}_3$ ),  $\text{KMnO}_4$ ,  $\text{K}_2\text{S}_2\text{O}_8$  [116–118],  $\text{K}_2\text{FeO}_4$ ,  $\text{Fe}(\text{NO}_3)_3$  [119],  $\text{KIO}_3$  [120],  $(\text{NH}_4)_2\text{S}_2\text{O}_8$ , sodium percarbonate [121], Oxone [122–124], citric acid, corrosion inhibitor (BTA) [125], Fenton reagent and other persulfates. Among them, the order of influence on MRR, from high to low, is as follows: persulfates, peroxides, potassium permanganate, peroxodisulfates,  $\text{O}_3$ , hydrogen peroxide, and so on [126–128]. However, based on the result form previous study, hydrogen peroxide is preferable since it forms harmless decomposition and by-products in the reaction. It is also revealed that in photo CMP (PCMP), the introduction of ultraviolet light can effectively generate oxidation agents like  $\text{O}_3$ , which is another approach for introducing oxidizer without worrying of distribution and oxidants stabilization [129].

**2.2.4. Mixed additives.** Mixed additives refer to the addition of various substances during the preparation of the polishing slurry to enhance its stability and polishing performance, aiming to achieve a high precision surface finish. Commonly used additives include pyridine hydrochloride, piperazine, imidazole, proline, arginine, glutamic acid, and pyridine carboxylic acid [130]. The results indicate that additives adsorb onto the surface of cerium oxide abrasives, affecting the interaction between the abrasive and silicon, thereby influencing the removal rate.

Research has indicated that after the addition of surfactants to ceria slurry, such as, poly-acrylic-acid, PEG, Sodium Dodecyl Benzene Sulfonate, Nonylphenol Ethoxylate, Cetyltrimethylammonium Bromide, the removal rate decreases with an increase in the concentration of surface-active agents [131]. According to Stokes' law of resistance [132], it can be inferred that a significant adsorption phenomenon occurring on the membrane surface leads to an elevation in local viscosity proximal to the surface. Consequently, this resultant layer functions as a protective barrier, impeding the approach of abrasive substances towards the membrane surface. Liu *et al* achieved a synergistic effect by incorporating hexagonal boron nitride (h-BN) as a lubricant with  $\text{CeO}_2$  abrasives, enhancing the lubricity and flowability of the slurry

[99]. As shown in figures 9(a) and (b), the subsurface damage layer of fused silica (FS) reduces after CMP. The surface roughness is only 0.124 nm. Figure 9(c) demonstrates that with the assistance of the lubricant h-BN, the movement of  $\text{CeO}_2$  abrasives shifts from sliding to rolling, preventing excessive surface abrasion caused by irregularly shaped  $\text{CeO}_2$  abrasives. This significantly reduces subsurface damage and greatly decreases surface roughness. In conclusion, the addition of additives aids in optimizing the removal mechanism, enhancing MRR and Ra, reducing the subsurface damage layer, and achieving a smooth, defect-free surface, meeting the requirements of ultra-precision manufacturing processes.

### 2.3. Physical characteristics of slurry

The flow rate, temperature, viscosity, and concentration of abrasives in the polishing slurry all affect the polishing results. A low slurry flow rate (SFR) can result in a high polishing temperature [133], aggregation of abrasives, leading to defects such as scratches and marks on the material surface after polishing. A high SFR reduces the polishing temperature, lowers the chemical removal rate, increases the mechanical removal rate, enabling quick material removal, but excessive flow rates may make it difficult to control the polishing depth, leading to potential over-polishing or uneven processing [134]. As the polishing slurry temperature increases, abrasives aggregate [3], friction coefficient of metal materials increases, MRR increases [135], but surface roughness also increases. For silicon dioxide ( $\text{SiO}_2$ ), with increasing polishing slurry temperature, the particle size of  $\text{SiO}_2$  abrasives decreases, zeta potential becomes more negative, resulting in a smoother silica surface [136]. Generally, with increasing slurry viscosity, MRR increases [137–139], but flowability of abrasives worsens, making the material surface more prone to scratching during polishing [140]. Lowering abrasive concentration improves the surface flatness of the CMP slurry [141]. When polishing  $\text{SiO}_2$  with  $\text{CeO}_2$  abrasive, the MRR decreases with increasing abrasive concentration due to the adsorption of  $\text{CeO}_2$  abrasives onto  $\text{SiO}_2$ , forming a broader adsorption layer on the silicon wafer surface [142]. Furthermore, the presence of water molecules in the environment also has an indispensable impact on the polishing of rare earth abrasives, with higher air humidity being more conducive to material removal [143].

### 2.4. Process parameters

The polishing results vary with different process parameters. Variations in abrasives, polishing slurry, grinding pressure, speed, time, polishing equipment, and polishing environment can lead to inconsistent polishing effects. The type, shape, and particle size of the abrasive also play a role in the final results. Therefore, in practical engineering, it is crucial to continually adjust and optimize these process parameters to identify the optimal combination, achieving the best polishing results to meet specific surface quality requirements for the workpiece. The summary of different polishing processes is listed in table 3.

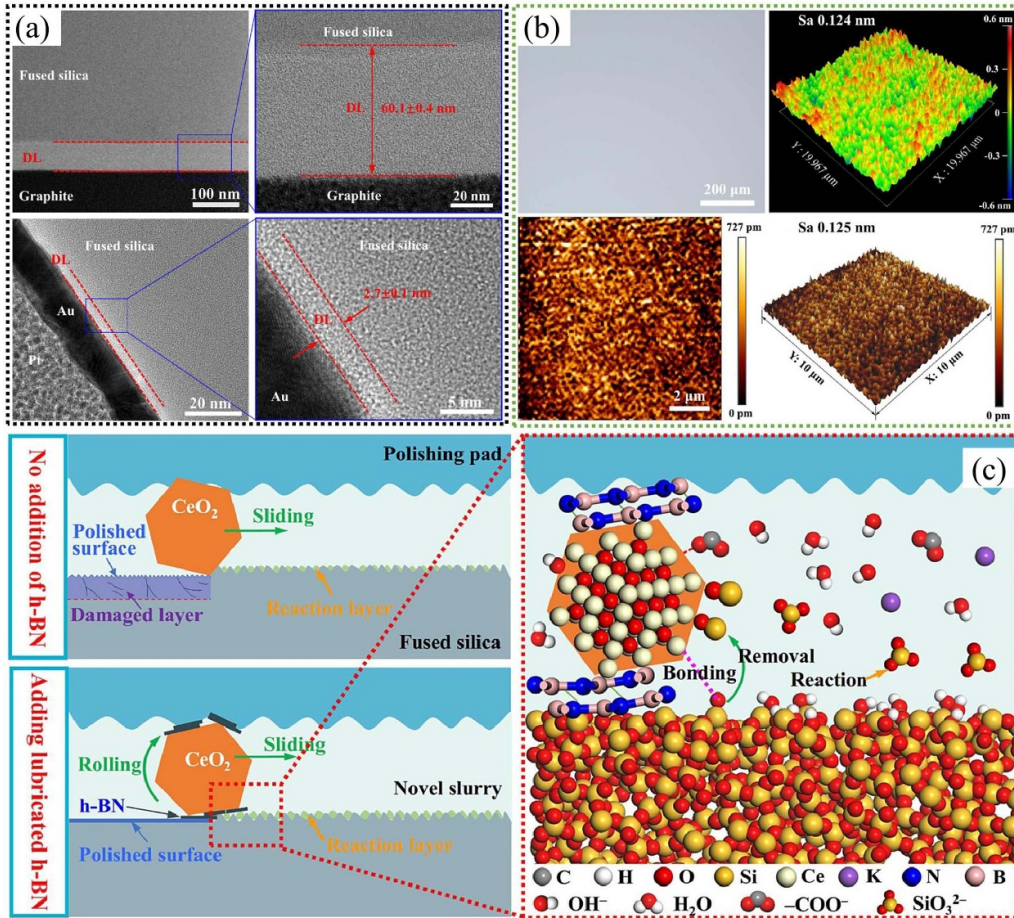


**Figure 9.** (a) Subsurface damage change and (b) surface morphology after polishing with novel developed CMP slurry. (c) Schematic diagram of CMP mechanism for FS using two types of CMP slurries. (a)–(c) Reprinted from [99], Copyright (2023), with permission from Elsevier.

**Table 3.** Summary of different types of rare earth abrasive polishing parameters.

Polishing pressure (kPa)	Pad speed (rpm)	Slurry flow rate (ml/min)	Polishing time (min)	Polished material	Ra/Sa/Rq/Sq (nm)	Measuring range ( $\mu\text{m} \times \mu\text{m}$ )	References
27.6	50	100	5	SiO <sub>2</sub>	Ra = 0.02	$5 \times 5$	[113]
30	160	5	NA	SiO <sub>2</sub>	Sa = 0.093	$20 \times 20$	[98]
23.8	87	300	1	SiO <sub>2</sub>	Sq = 0.45	$10 \times 10$	[144]
20.7	87	120	1	SiO <sub>2</sub>	Ra = 0.183	$5 \times 5$	[145]
27.6	93	150	1	SiO <sub>2</sub>	NA	NA	[42]
200	80	NA	90	SiO <sub>2</sub>	Rq = 0.52	$5 \times 5$	[146]
20	90	100	1	SiO <sub>2</sub>	Ra = 0.36	$5 \times 5$	[147]
109.28	80	25	3	SiO <sub>2</sub>	Ra = 0.36	$5 \times 5$	[19]
27.6	40	50	0.33	STI	NA	NA	[45]
15	60	8	15	Cu	Sa = 0.099	$50 \times 50$	[140]
6.9	93	90	3	Cu	Ra = 0.363	$5 \times 5$	[106]
14.5–21.3	30–110	1.5	10	4 H-SiC	Sa = 0.084	$1 \times 1$	[148]
27.6	90	90	20	6 H-SiC	Ra = 0.11	$2 \times 2$	[101]
33	150	50	20	Al <sub>2</sub> O <sub>3</sub>	Ra = 0.52	$5 \times 5$	[74]

NA (Not available) Cu, 4 H-SiC, 6 H-SiC, Al<sub>2</sub>O<sub>3</sub> (Single crystal) SiO<sub>2</sub> (Amorphous).

The typical flat polishing device is displayed in figure 10(a). With the rotation of the polishing pad, the sample attached under the pressure plate undergoes the effects of friction with

abrasives in the polishing slurry and reacts with the chemical components in the polishing slurry. Through the combined action of these factors, the material removal effect is achieved.

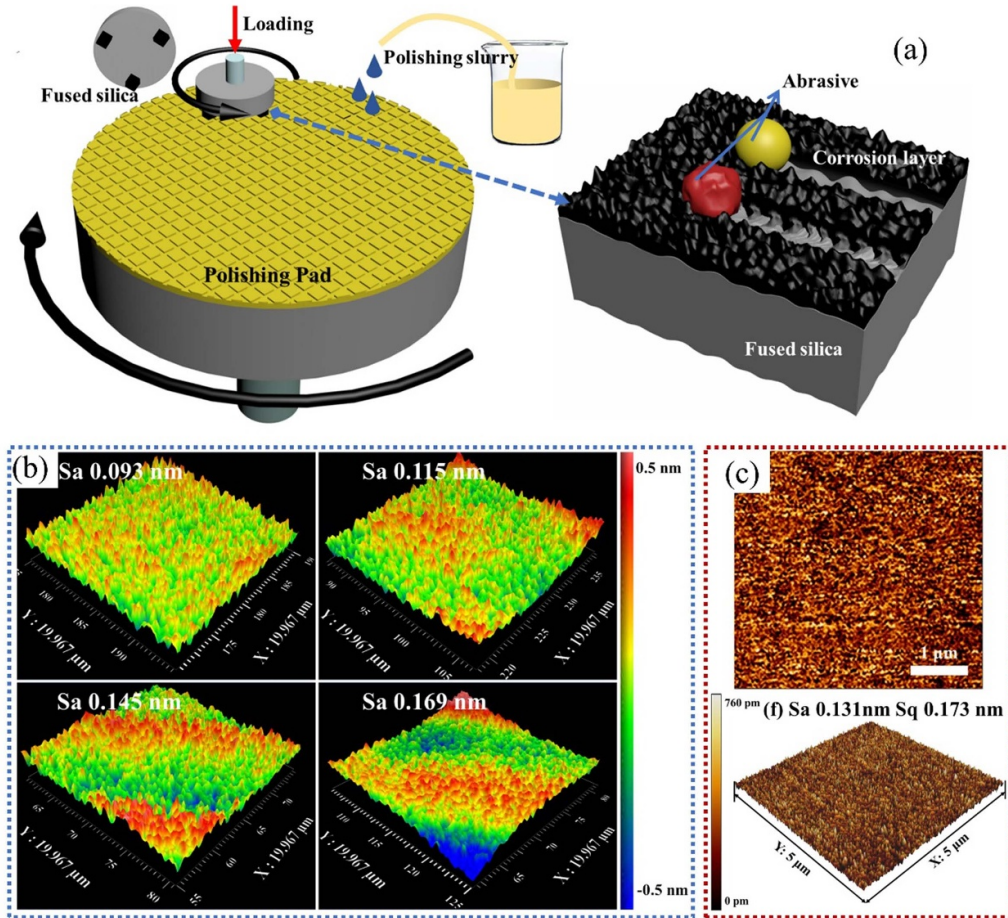


**Figure 10.** (a) Schematic diagram of CMP process and abrasive scratch. (b) Surface morphology of FS after polishing using various  $\text{CeO}_2$  abrasives. (c) AFM 2D, 3D images of fused silica polished with  $\text{CeO}_2$  abrasives. (a)–(c) Reprinted from [98], Copyright (2023), with permission from Elsevier.

Recently, Xu *et al* employed a hydrothermal method to prepare nanoscale  $\text{CeO}_2$  abrasives with uniform shape [98]. The atomic force microscopy (AFM) images reveal the attainment of an atomic-scale surface with a surface roughness  $S_a$  of 0.093 nm after polishing, as depicted in figures 10(b) and (c). Their research indicates that the key to obtaining a smooth FS surface lies in the  $\equiv\text{Ce}-\text{O}-\text{Si}\equiv$  structure formed through a chemical tooth action. Several studies have demonstrated that combining thermal oxidation pretreatment with soft abrasive polishing can effectively achieve damage-free and atomically smooth polishing of the carbon surface of 4H-SiC [149]. However, it is important to note that high oxidation temperatures may result in the formation of micro-pits during the polishing process, necessitating further optimization of surface modification techniques.

When varying amounts of hydroxyl (OH) groups are introduced onto the surface of FS, the removal rate of surface atoms exhibits an initial increase with increasing hydroxylation degree, followed by a subsequent decrease. The interfacial pressure exerts influence on both the quantity and manner in which atom removal occurs. As pressure increases, the mode of removal transitions from single-atom elimination to chain

removal. This finding serves as a crucial theoretical foundation for elucidating the atomic-level mechanism underlying FS removal in CMP [150]. Zhao *et al* proposed a new cross-scale model from millimeter to nanometer scale, enabling the analysis of system logic mapping across macro, meso, micro, and nano scales. This study provides valuable insights for the design and development of CMP processes [151]. Future research should focus on exploring the potential influence mechanism of rare earth elements on CMP.

In this subsection, it can be seen that the influence of slurry compositions as well as their concentration is important to the performance of the polishing process. Rare earth abrasives like ceria mainly provided the core chemical mechanical removal mechanism and the core mechanism is very sensitive to other conditions. For examples, the change of pH and temperature would greatly promote or impede the chemical reaction, while the viscosity as well as the dispersibility of the abrasives have determined effect on the mechanical removal process. Therefore, the investment into the development of new ceria abrasives is equally important to the analysis and development of slurry composition, while the latter one is often much easier and cheaper.

### 3. Research on typical materials

Due to the special reaction mechanism between element Si and Ce, ceria abrasives have been extensively used in polishing materials with Si elements, which are mainly monocrystalline silicon, all kinds of silicate glass, FS, SiC and so on [152]. However, the material removal mechanism varies from material to material since the structure and the bond strength are very different for these materials. In this chapter, with the help of different additive in the rare earth element based polishing slurry, new polishing mechanism has been continuously reported for different materials.

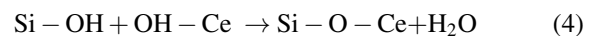
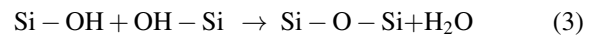
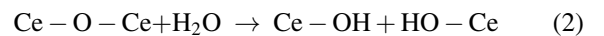
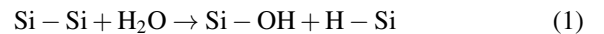
Research on different materials generally requires the adoption of specific methods to elucidate. For instance, post-polishing, material characteristics such as surface morphology, roughness, elemental composition, functional groups, and changes in molecular structure need to be investigated [153, 154]. Methods for obtaining information about material structure and elemental composition include x-ray photoelectron spectroscopy (XPS), Raman spectra, Fourier transform infrared spectroscopy (FTIR), x-ray diffractometer (XRD), energy dispersive spectrometer, and so on [155]. First principal simulation, molecular dynamic (MD) simulations are also conducted to study the material removal mechanism behind CMP [156–159]. However, there is still a big gap between macro scale polishing process and the nano scale or even atomic scale material removal process. The combination of testing like XPS, XRD and FTIR with the MD simulation is a viable solution for revealing part of the mechanism by verifying the resultant composition, there is still much to be done for revealing the mechanism.

#### 3.1. Silicon (Si)

Si is widely utilized in integrated circuits, semiconductors, and the microelectronics industry due to its narrow bandgap of 1.11 eV, intact crystal lattice structure, exceptional thermal oxidation performance, high carrier mobility, and low defect density [160–162]. As the size of silicon-based components continues to decrease, there is a corresponding increase in the surface-to-volume ratio, highlighting the growing significance of surface quality on physical and chemical properties. Consequently, precision components necessitate an ultrasmooth surface and a low-damage layer. In the Si manufacturing processes, CMP is typically chosen as a crucial step towards achieving high-quality surfaces.

In order to explore the polishing mechanism of  $\text{CeO}_2$  on the surface of Si, Cui *et al* developed a cerium dioxide-based polishing slurry [163]. After CMP, the surface is smooth, free from impurities and scratches, and the Sa measures 0.067 nm as shown in figures 11(a) and (b). The transmission electron microscopy (TEM) images in figure 11(c) reveal the effective removal of the non-uniform damage layer on the surface of single crystal silicon, leading to a significant improvement in surface quality. Moreover, a reduction in subsurface damaged layer is observed, resulting in the attainment of a sub-Ei surface for single crystal silicon. Through simulation study of the CMP mechanism (figure 11(d)), combined with experimental

results, the mechanism of the chemical reactions is shown in equations (1)–(4):



The objective of removing the surface material of silicon is achieved through the breakage of Si–O–Ce bonds. Subsequently, newly exposed silicon atoms continue to react upon contact with the polishing solution. Through this cyclic process, the removal of single-crystal silicon at the atomic level is ultimately achieved.

The mechanical removal mechanism of Si changes according to the distinct exposed surfaces of  $\text{CeO}_2$ . Some research propose that adhesive wear is the dominant form of wear between Si and  $\text{CeO}_2$ . The relationship between the friction force of Si and  $\text{CeO}_2$  is as follows:  $F(\text{CeO}_2(111)) > F(\text{CeO}_2(110)) > F(\text{CeO}_2(100))$ . The wear rate of  $\text{CeO}_2$  and its ability to remove Si during the CMP process are as follows:  $WR(\text{CeO}_2(111)) > WR(\text{CeO}_2(110)) > WR(\text{CeO}_2(100))$  and  $RR(\text{CeO}_2(111)) > RR(\text{CeO}_2(100)) > RR(\text{CeO}_2(110))$ . Consequently, it can be deduced that the  $\text{CeO}_2(111)$  surface is the predominant crystal surface prone to experiencing wear and demonstrates exceptional ability in removing Si due to its high friction force and greater hardness. Maybe because of the high surface energy, the Si removal ability of  $\text{CeO}_2(110)$  surface is poor [164]. Experiments have shown that the  $\text{CeO}_2(111)$  surface may form a greater number of Si–O–Ce bonds, while on the  $\text{CeO}_2(100)$  surface, due to lower coordination, stronger bidentate bonds with silicon can be formed by the Ce atoms. Despite having fewer Si–O–Ce bonds than the  $\text{CeO}_2(111)$  surface, the stronger bonding on the  $\text{CeO}_2(100)$  surface compensates for this and results in almost identical removal rates. This could potentially explain why practical CMP processes show higher polishing efficiency on the  $\text{CeO}_2(100)$  surface [165].

#### 3.2. FS

The CMP of silica-based glasses is a pivotal technology for achieving surface planarization and producing defect-free, ultra-smooth glass surfaces, which are indispensable for various applications including optical glasses, liquid crystal displays, display panels, window panes, precision glass lenses and glass magnetic memory disks. FS is preferred for numerous high-performance optical elements because of its exceptional optical properties and remarkable resistance to chemical, thermal, and radiation effects [166, 167]. However, its hard and brittle nature has historically limited precise machining and manufacturing processes [168]. Achieving ultra-high surface quality on FS optical surfaces efficiently remains challenging. Nevertheless, CMP technology has been employed in FS treatment, leading to significant advancements in meeting the stringent surface quality standards of FS [169]. The

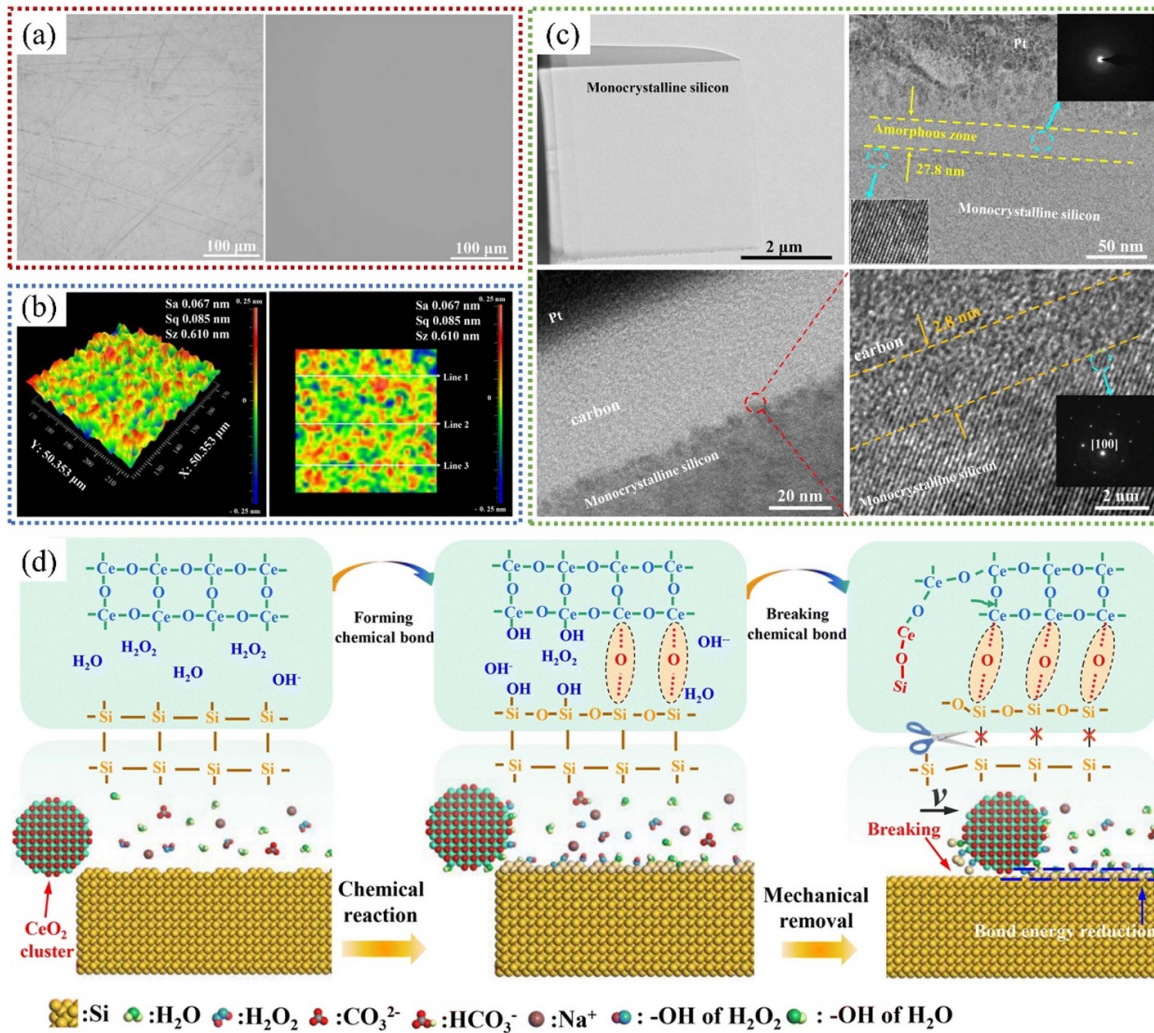
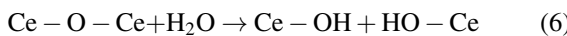
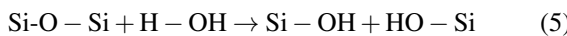
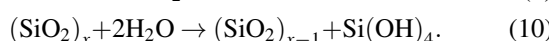
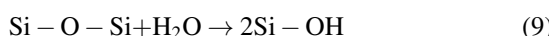


**Figure 11.** (a) SEM images of single-crystal silicon surface before and after CMP. (b) Surface roughness of the polished samples, (c) TEM images of the single-crystal silicon surface after CMP. (d) Single-crystal silicon CMP mechanism. (a)–(d) Reproduced from [163] with permission from the Royal Society of Chemistry.

main component of FS is SiO<sub>2</sub>. When using a slurry containing CeO<sub>2</sub> abrasive for polishing the SiO<sub>2</sub> surface, the primary chemical reactions as indicated by equations (5)–(7) [50]:



In the polishing of FS glass [67–69], it has been proposed that SiO<sub>2</sub> materials may undergo hydration reactions when they come into contact with OH<sup>-</sup> in alkaline slurries [67]. XPS analyses have further confirmed the presence of Si–O, Si–O–Si, and Si–OH bonds on the surfaces of FS immersed in alkaline solutions [170]. The formation of hydration and Si–OH on SiO<sub>2</sub> surfaces as illustrated in equations (8)–(10):



At present, researchers have developed various MDs programs to simulate the CMP process. The MDs method is a key technique for studying the mechanochemical reactions of CeO<sub>2</sub> abrasives during the CMP process on SiO<sub>2</sub> surfaces [171]. A comprehensive analysis and discussion have been conducted on the atomic-level phenomena in CMP, such as bond breaking and formation, as well as the dynamics of electronic states and electron transfers. It has been discovered that the applied mechanical force significantly enhances the chemical reactions at the CeO<sub>2</sub>–SiO<sub>2</sub> interface [165]. Moreover, it is possible to observe the electron state transition from Ce<sup>4+</sup> to Ce<sup>3+</sup>. The concentration of Ce<sup>3+</sup> and oxygen exchange capacity significantly influence the polishing efficiency when using cerium-based polishing slurry for polishing SiO<sub>2</sub> [172]. Kim *et al* utilized a hydrothermal technique to synthesize ceria NPs, incorporating varying concentrations of lanthanide elements (La and Nd) as dopants in order to enhance the presence of Ce<sup>3+</sup> [59]. The incorporation of trivalent lanthanide ions into ceria induced the generation of oxygen vacancies, causing the conversion of adjacent Ce<sup>4+</sup> to Ce<sup>3+</sup> through reduction. By

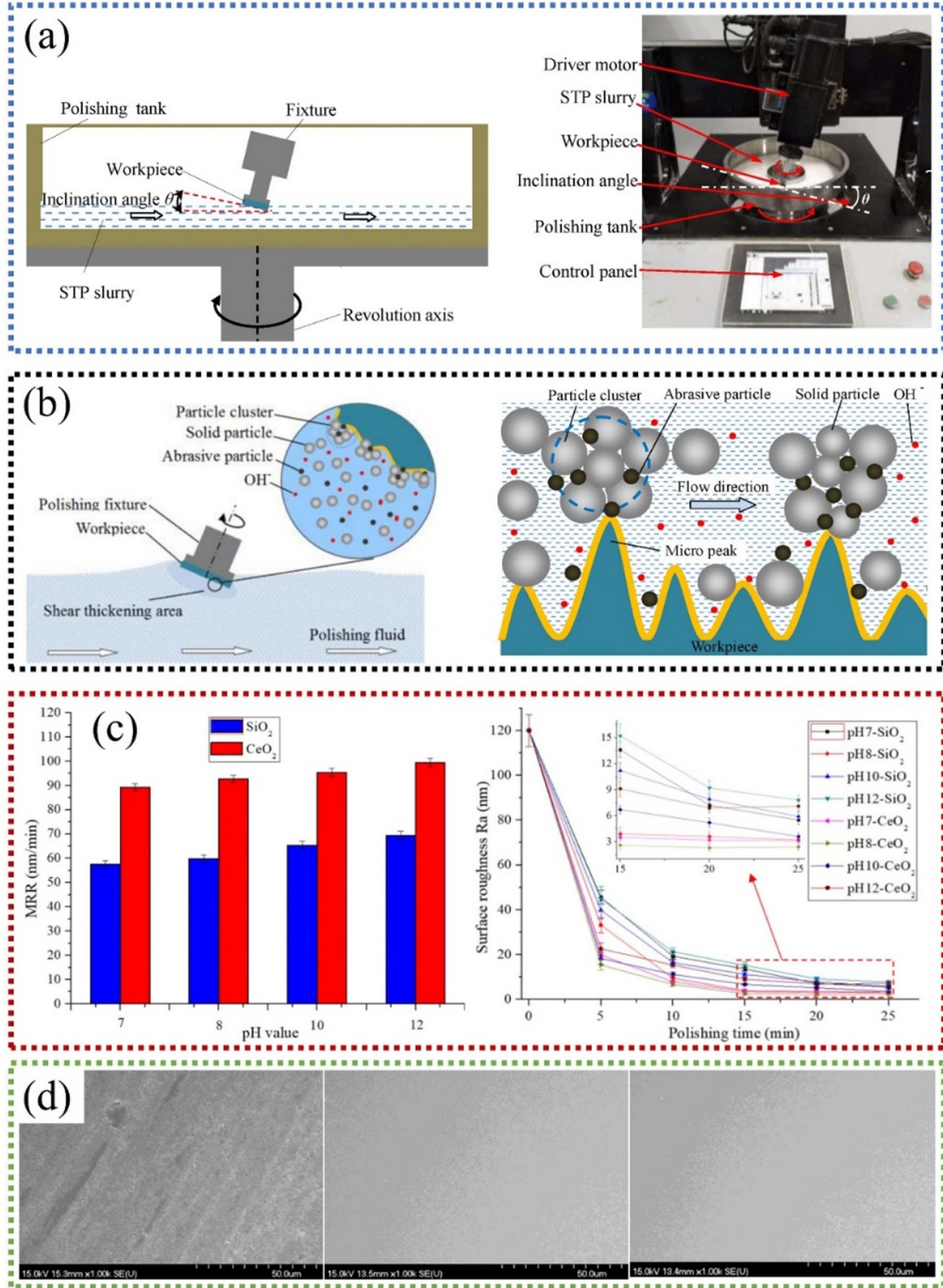


**Figure 12.** The experimental (a) device and (b) material removal mechanism schematic of the STP. (c) The variation of MRR and Ra with different pH values. (d) The surface morphology before and after polishing. (a)–(d) Reproduced from [173]. CC BY 4.0.

increasing the dopants content, particularly Nd, there was an observed increase in the concentration of  $\text{Ce}^{3+}$ . The outcomes demonstrated that La and Nd-doped cerium dioxide exhibited a remarkable MRR, indicating that elevating the concentration of  $\text{Ce}^{3+}$  can yield an exceptionally smooth  $\text{SiO}_2$  surface with a Ra value measuring 0.135 nm.

Relying on shear thickening polishing (STP) technology with non-Newtonian power-law fluids enables efficient and high-quality polishing of FS. Shao *et al* used  $\text{SiO}_2$  and colloidal  $\text{CeO}_2$  as abrasives to polish FS [173]. The experimental

device and schematic of the STP can be seen in figures 12(a) and (b), respectively. Different clamping forces are exerted on abrasives by solid abrasives at varying shear rates, significantly enhancing the force acting on them and accelerating MRR. Figure 12(c) demonstrates that increasing the pH value of the polishing slurry leads to an increase in MRR, while initially decreasing and then increasing surface roughness of FS. A preferable surface roughness is achieved when the pH value is set at 8. The surface morphology before and after polishing is depicted in figure 12(d), resulting in a decrease from

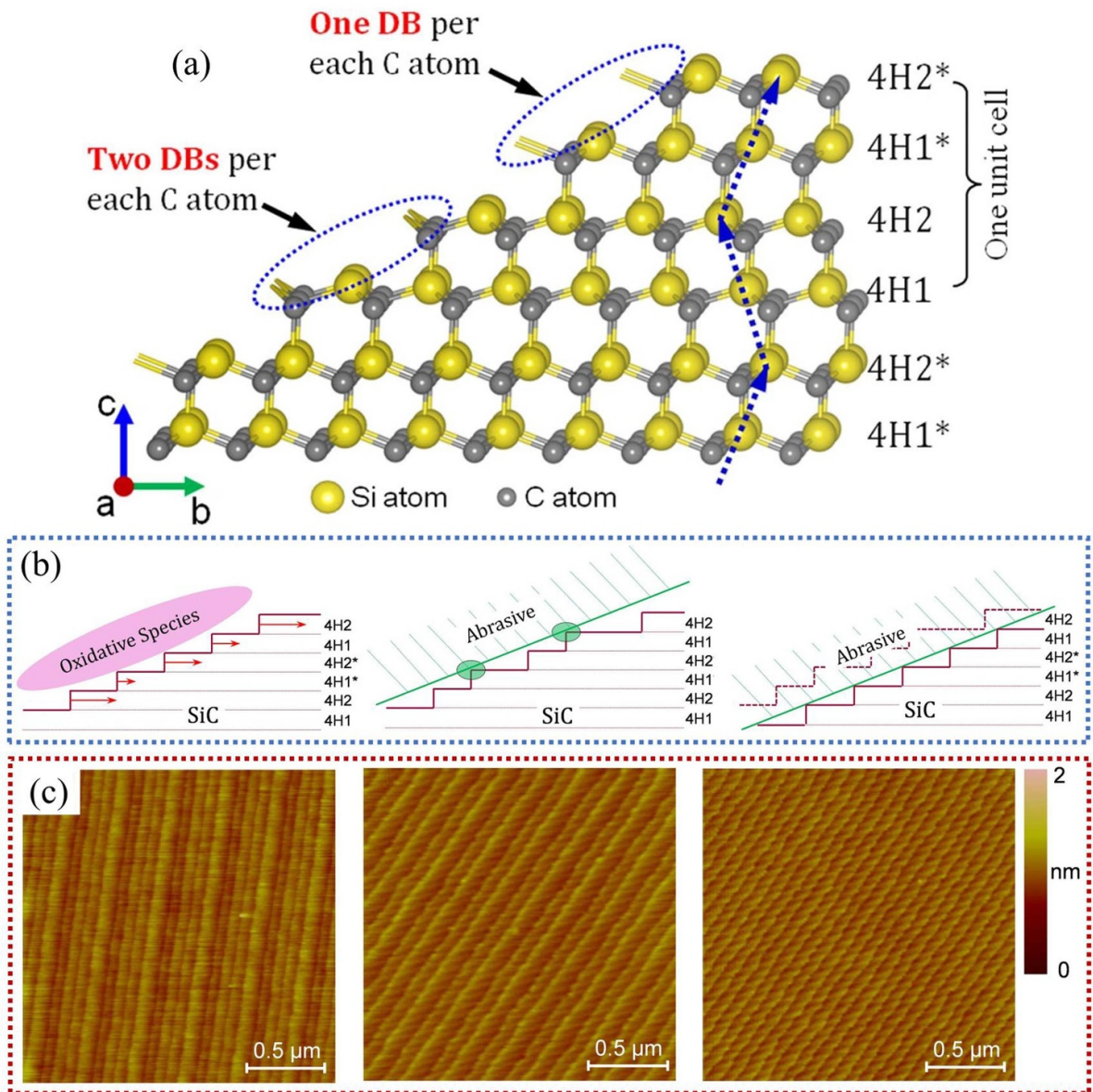


**Figure 13.** (a) Crystal structure of 4 H-SiC. (b) Generation mechanism of step-terrace structure of 4 H-SiC. (c) Variation of surface terrace-step structures of polished SiC with increasing polishing pad rotation speed by AFM. (a)–(c) Reproduced from [183]. CC BY 4.0.

an initial Ra of  $120 \pm 10$  nm to a final Ra of 2.3 nm and 2.1 nm, accompanied by MRR values of 121.6 nm/min and 126.2 nm/min, respectively.

The esthetic appearance of all-ceramic restorations has led to their widespread utilization in dentistry. One of these materials is lithium disilicate glass ceramic ( $\text{Li}_2\text{Si}_2\text{O}_5$  or  $2\text{SiO}_2 - \text{Li}_2\text{O}$ ), with its main component being 57%–80% silica [174]. Research has revealed the presence of silica in the solution in which lithium disilicate samples are soaked. Therefore, polishing with  $\text{CeO}_2$  can be employed, where the polishing process primarily involves chemical reactions with  $\text{SiO}_2$ , ultimately yielding a smooth ceramic surface. This represents a novel approach for polishing lithium disilicate glass ceramics, pointing out a new direction for achieving atomic-level precision manufacturing of all-ceramic restorations using rare earth abrasives in the future [175].

### 3.3. Silicon carbide (SiC)

SiC has emerged as a highly promising semiconductor material for applications that require exceptional electric performance in terms of high power and high frequency. This is attributed to its outstanding characteristics, including a wide band gap, excellent thermal conductivity, high heat resistance, remarkable temperature stability, and favorable crystal lattice arrangement with GaN [176–178]. However, the challenge lies in achieving significant removal rates on the surface of SiC substrates due to their elevated mechanical hardness and pronounced chemical inertness [179–182].

The crystal structure of 4H-SiC in figure 13(a), contains four silicon–carbon bilayers in a unit cell of 4H-SiC single crystal. When polishing SiC with  $\text{CeO}_2$  slurry, as shown in figures 13(b) and (c), with the increase of polishing pad

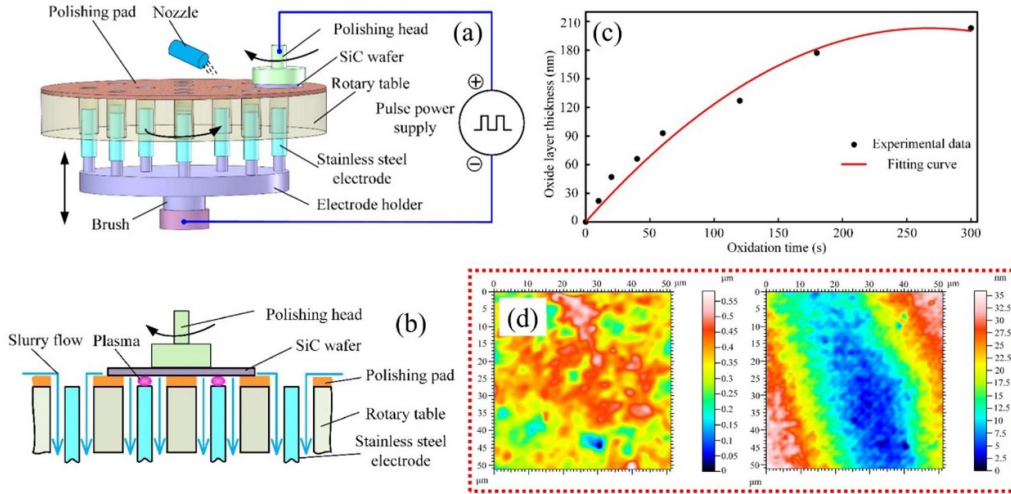


**Figure 14.** The experimental (a) device and (b) polishing details schematic of the AOMP. (c) The change in thickness of the oxide layer over time. (d) Images of SWLI after treatment with different anodizing time and 5 min of CMP. (a)–(d) Reprinted from [184], Copyright (2020), with permission from Elsevier.

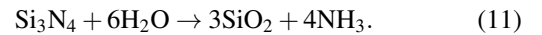
rotation speed, the stepped structure on the surface of SiC substrate changes accordingly, transitioning from the a–b–a<sup>\*</sup>–b<sup>\*</sup> type to the a–b type, and then to a uniform a–a type, presenting three structural morphologies. The MRR also increases accordingly [183].

For polishing SiC, electro CMP (ECMP) has emerged as a relatively mature technological solution, which will be elaborated on in section 4. Apart from ECMP, there are also other methods available for polishing SiC. Yin *et al* proposed a novel polishing technique that combines anodic oxidation and mechanical polishing (AOMP) [184]. Schematic diagram of the AOMP experimental device as illustrated in figures 14(a) and (b), the device comprises of an anodic oxidation system and a mechanical polishing unit, collaborating harmoniously to attain a SiC surface that is both sleek and even. The significant growth of the oxide layer during the initial phase of oxidation can be observed in figure 14(c). Subsequently, a decrease in the anodic oxidation rate leads to a reduction in the formation rate of oxide layer thickness. The impact of controlling the levels of anodic plasma oxidation rate and CMP rate was investigated to analyze their effects on polishing outcomes. Experiments showed that when the two rates were close, the minimum roughness of 1.06 nm could be obtained (figure 14(d)).

#### 3.4. Silicon nitride ( $\text{Si}_3\text{N}_4$ )

The shallow trench isolation (STI) polishing process is a specific CMP application that typically involves the selectively eliminating silicon dioxide and silicon nitride on a patterned wafer substrate [185–188]. In this scenario, the etched trenches are filled with a dielectric material (such as silicon dioxide) and polished using the silicon nitride barrier film as a stop layer. The final step of the process involves removing the silicon dioxide from the barrier film while minimizing any removal of exposed silicon nitride and trench silicon dioxide. This necessitates the use of a high selectivity slurry capable of

achieving a high relative ratio between removal rates of silicon dioxide material and silicon nitride [189–192]. Aqueous solutions readily induce  $\text{Si}_3\text{N}_4$  surface hydrolysis reactions, resulting in ammonia liberation and generation of  $\text{SiO}_2$ -like surface structures. Such hydrolysis reactions can be represented by the following equation (11).



Additionally, in high-temperature environments ( $>200^\circ\text{C}$ ),  $\text{CeO}_2$  abrasives can undergo a direct chemical reaction (redox reaction) with  $\text{Si}_3\text{N}_4$  materials [193], resulting in the generation of  $\text{SiO}_2$  and  $\text{N}_2(\text{g})$ , as illustrated in equation (12). Elevating the temperature has been demonstrated to confirm that  $\text{CeO}_2$  is only stable at low temperatures [194],



when  $T > 200^\circ\text{C}$

It is discovered that the removal mechanism of polishing  $\text{Si}_3\text{N}_4$  material involves the formation of  $\text{SiO}_2$  on its surface. The  $\text{SiO}_2$  formed through further polishing eventually reaches the desired surface polishing level. When using slurry containing  $\text{CeO}_2$  abrasive for polishing STI, the diverse decomposition performance of ionic surfactants in the slurry can affect the stability of the slurry and the variation of abrasive particle size at different pH levels. Experimental results indicate that at high pH levels, the particle size distribution of  $\text{CeO}_2$  is more stable and uniform, reducing the number and depth of scratches on the surfaces of  $\text{SiO}_2$  and  $\text{Si}_3\text{N}_4$  during polishing [195–197]. There are studies on the impact of  $\text{CeO}_2$  abrasive particle size on STI CMP and have identified the optimal abrasive size to achieve maximum removal selectivity between oxide and nitride films, realizing atomic-level polishing of STI [198].

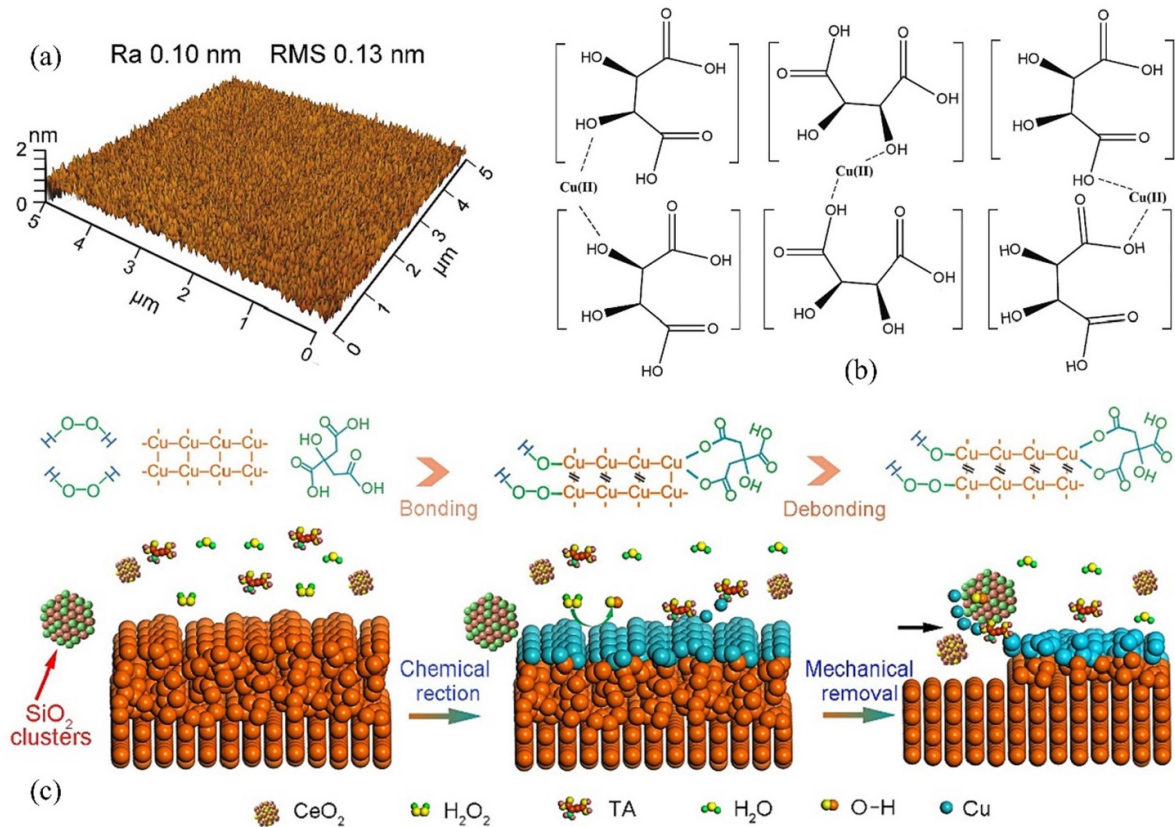


**Figure 15.** (a) 3D-AFM images of copper surface after CMP. (b) Chelation reaction between copper ions and tartaric acid. (c) Mechanism of copper CMP in the novel green polishing slurry. (a)–(c) Reprinted from [122], Copyright (2023), with permission from Elsevier.

### 3.5. Copper

Over the last twenty years, the CMP technique applied to copper (Cu) substrates has undergone significant evolution, transitioning from the Damascus process to the integration of barrier layers within Cu interconnects [199]. In recent years, there has been a growing consensus among researchers that surface defects and MRRs in Cu are closely tied to the properties of the polishing slurry. Consequently, considerable effort has been focused on scrutinizing the impact of various compositional factors within the slurry on Cu-CMP parameters [200].

Rare earth abrasives are applied in the precision grinding and CMP polishing of copper. Core-shell composite abrasives play a crucial role in copper CMP processes due to their unique advantages of adjustability and synergistic performance, reducing the number of deep scratches and pits caused by mechanical actions. In order to investigate the fundamental processes involved in material removal and planarization, a quantitative analysis is conducted on the nanoscratching behavior of copper film. Researchers utilized a nanoindenter system equipped with a custom-made CeO<sub>2</sub> tip, examining both constant load and ramp load modes. The detailed examination revealed that adjusting the normal force parameter and abrasive particle size can accurately predict the MRR [201]. Chen *et al* prepared polystyrene/cerium dioxide (PS/CeO<sub>2</sub>) abrasives to polish copper, achieving a surface close to an Ai-level

and proved that the potential CMP application of composite abrasives for challenging materials like copper and low-k dielectric materials [202]. SiO<sub>2</sub>/CeO<sub>2</sub> composite abrasives with different sizes of SiO<sub>2</sub> microspheres were prepared by Shi *et al* it is found that the surface roughness and MRR results are different with the change of abrasive size [106]. In traditional CMP, highly corrosive slurries such as strong acids and bases are primarily used, which can easily cause environmental pollution. Therefore, using green and eco-friendly polishing slurry to achieve atomically smooth surfaces is a major challenge currently faced. To address this issue, Liu *et al* developed a novel green CMP slurry for polishing copper surfaces [122]. They used cerium dioxide and silicon dioxide as composite abrasives, with tartaric acid serving as a pH adjuster. This approach successfully achieved a surface with a Ra of 0.1 nm, as shown in figure 15(a). The chelation product of copper ions with tartaric acid is illustrated in figure 15(b). Figure 15(c) reveals the polishing mechanism, where an adsorbed layer of copper oxides (CuO and Cu<sub>2</sub>O) and chelates forms on the copper surface and is subsequently removed. Ultimately, an atomic-level copper surface was obtained.

Oxygen-free copper (OFC) serves as a core component in high-end manufacturing with stringent surface quality requirements [203]. Achieving high-quality atomic-level surfaces has always been a significant challenge. Liu *et al* prepared well-dispersed SiO<sub>2</sub> NPs and developed a CMP slurry

composed of  $\text{SiO}_2$  NPs,  $\text{CeO}_2$  NPs,  $\text{H}_2\text{O}_2$ ,  $\text{NaHCO}_3$ , polyaspartic acid, and deionized water [105]. After CMP, the average roughness of OFC wafers reached 0.092 nm, achieving atomic-level surfaces of OFC. The present study proposes a novel approach for investigating the atomic-level polishing of Cu in future research.

### 3.6. Sapphire ( $\alpha\text{-Al}_2\text{O}_3$ ) wafer

The single crystal sapphire ( $\alpha\text{-Al}_2\text{O}_3$ ) substrate exhibits outstanding optical and mechanical characteristics, encompassing electrical and dielectric properties, hardness, and resistance to chemical corrosion [204]. Additionally, it boasts high infrared transmittance, remarkable wear resistance, and superior stability at elevated temperatures. Consequently, the use of  $\alpha\text{-Al}_2\text{O}_3$  has experienced a significant increase in cutting-edge areas like solid-state lasers, infrared windows, semiconductor chips, missile enclosures, and see-through protective shields [205]. Nevertheless, its formidable attributes, including high hardness (scoring 9 on the Mohs scale), brittleness, and chemical inertness, pose challenges in achieving sapphire wafers with the requisite surface smoothness [206]. As a crucial technique for sapphire polishing, CMP effectively regulates both the overall and localized surface smoothness during processing [207–209].

In order to delve into the polishing mechanism and interfacial contact behavior between abrasives and sapphire, Xu *et al* synthesized a novel  $\text{CeO}_2$ -coated diamond composite abrasive, which effectively reduced the surface roughness of sapphire and increased the MRR [38]. Zhou *et al* utilized PS with  $\text{CeO}_2$  and detonation nanodiamond (DND) to synthesize three types of core–shell abrasives [74]. Among them, the surface quality of sapphire polished using  $\text{PS@CeO}_2/\text{DND}$  exhibited superior characteristics. Chemical reactions inferred from the obtained XPS data are depicted as follows equations (13)–(15):



Through analysis of the polished sapphire surface and worn debris, concluded that the enhanced polishing performance is attributed to the solid-phase reaction between  $\text{CeO}_2$  and sapphire, as well as the mechanical removal effect of the composite abrasive.

From the above analysis, it can be concluded that the core chemical reaction between ceria abrasive and materials that contains Si element is the same. However, due to the different chemical activeness of other elements, the chemical reactions that happens in the polishing process as well as the final removal mechanism is vastly different. As a result, polishing slurry must be developed according to the material being polished and for difficult to machine materials like SiC and  $\text{Si}_3\text{N}_4$ , energy field assistant is often crucial for an acceptable MRR.

## 4. Rare earth abrasive energy field assisted polishing

The core concept of CMP is to first create a surface modification layer, which is softer and can be easily removed. There are many energy fields that can accelerate this process or modified the surface on their own. Therefore, energy field assistance has been considered an effective way of promoting surface quality and MRR. For decades, research have been conducted to develop novel polishing device integrates rare earth abrasives to further improve polished surface roughness and efficiency. In this section, CMP with the assistance of different types of energy fields are reviewed, including PCMP, ECMP, photoelectrochemically combined mechanical polishing (PECMP), and plasma assisted polishing (PAP). The core mechanism of these assistive technologies is briefly introduced. And the advantages and disadvantages of each assistive technology, as well as the surface quality achieved when polishing different materials with rare earth abrasives in each energy field, are summarized in table 4. It can be observed that when using rare earth abrasives as polishing abrasives, PCMP technology is primarily used for polishing  $\text{SiO}_2$ , while ECMP, PECMP, and PAP technologies are mainly used for polishing SiC. Among these, PAP technology achieves lower surface roughness for SiC. PCMP and ECMP technologies have high MRRs and polishing efficiency.

Overall, for typical materials, ECMP and PECMP typically have higher polishing efficiency, followed by PCMP, with PAP being the lowest. However, for hard materials and complex components, although PAP has lower polishing efficiency, it can achieve higher precision in surface quality. It is worth noting that introducing energy fields in the polishing process requires careful consideration of the potential environmental impacts. The leftover electrolyte from the polishing equipment in ECMP must be treated harmlessly. Comprehensive management of chemicals along with light and electrical energy in PECMP is required. Any residual gases produced by PAP equipment should be promptly treated. This is not only to prevent environmental pollution but also to ensure personal safety.

### 4.1. PCMP

PCMP technology is widely used in the ultra-precision machining of high-hardness and chemically inert materials, such as GaN and SiC, addressing the challenge of low MRRs. In PCMP [221, 222], the use of ultraviolet (UV) radiation and photocatalysts can increase the concentration of active oxygen species (such as hydroxyl radical  $\bullet\text{OH}$ , superoxide radical  $\bullet\text{O}_2^-$ ) and photogenerated holes  $\text{h}^+$  [67], as depicted in figure 16. This phenomenon accelerates the formation of the material's surface oxide layer, contributing to an improvement in MRR.

Using the same  $\text{CeO}_2$ -containing polishing slurry for CMP (without UV irradiation) and PCMP (with UV irradiation) treatment on  $\text{SiO}_2$  surfaces [69]. AFM analyses confirmed that the resulting RMS roughness values were  $0.18 \pm 0.01$  nm and  $0.17 \pm 0.01$  nm, respectively. Figures 17(a)–(c) demonstrates

**Table 4.** Comparison of different energy field-assisted polishing processes.

Polishing process	Advantages	Disadvantages	Polished material	Ra/Sa/RMS (nm)	References
PCMP	· Precise control of material removal	· Requires specialized light sources	SiO <sub>2</sub>	Ra = 0.132	[210]
	· Enhanced surface smoothness	· Limited penetration depth of UV light	SiO <sub>2</sub>	Ra = 0.137	[67]
	· Can be used on non-conductive materials	· Potential degradation of photoresist materials	SiO <sub>2</sub>	Ra = 0.12	[68]
ECMP	· High MRR	· Complex setup and control requirements	SiC	Sa = 0.853	[212]
	· Improved surface finish quality	· Potential for electrochemical corrosion	SiC	Ra = 0.51	[75]
	· Reduced mechanical stress on the workpiece	· Limited to conductive materials	SiC	Ra = 0.5	[213]
PECMP	· Combines benefits of PCMP and ECMP	· Very complex process control	SiC	Sa = 0.084	[214]
	· High precision and surface quality	· Requires both light and electrical energy sources	SiC	RMS = 0.23	[215]
	· Effective for both conductive and non-conductive materials	· Higher operational costs			
PAP	· Can process complex geometries	· Expensive equipment and operational costs	SiC	Ra = 0.277	[216]
	· Improved surface integrity and cleanliness	· Potential for surface damage due to plasma exposure	SiC	RMS = 0.3	[217]
	· high controllability	· Requires vacuum environment	SiC	RMS = 0.1	[218]
			SiC	RMS = 0.28	[219]
			SiC	RMS = 0.1	[220]

NA (Not available) RMS (Root mean square).

that both CMP and PCMP applications using these composite abrasives yielded smooth surfaces without any noticeable scratching grooves, etching pits, or residual NPs. However, cross-sectional analysis in figures 17(d)–(f) confirms that PCMP conditions contribute to reducing topographical variations, ensuring that the shape of silicon dioxide remains unchanged after polishing, enhancing shape accuracy.

In addition to the above research, novel carbon-coupled CeO<sub>2</sub> heterostructures were developed by Wang *et al* as functional abrasives for the PCMP system [68]. As shown in the figures 18(a)–(c), surface modification occurs after the contact of CS/CeO<sub>2</sub> with oxides. The relative movement and mechanical action between the abrasive and the hydration layer cause the relatively weak Si–O–Si bonds to break, effectively removing materials during the CMP/PCMP process. From figures 18(d) and (e), it can be observed that Y-doping modification can generate more oxygen Vo and Ce<sup>3+</sup> on the surface of CeO<sub>2</sub>, as well as the effective separation of e<sup>-</sup>/h<sup>+</sup> pairs, both of which play a crucial role in enhancing photocatalytic oxidation activity.

In general, PCMP is effective in lowering the surface roughness and boosting the MRR especially for inert materials. However, the integration of the UV light into the polishing equipment is very important since the effectiveness of UV radiation on the slurry and on the polishing zone can be very different. As for the surface roughness, there is no substantial evidence that PCMP can help achieve an atomic roughness

in its current state. Therefore, it is necessary for us to further deepen our research on PCMP to achieve atomic-level manufacturing.

#### 4.2. ECMP

Recently, there has been a significant focus on enhancing the efficiency of material removal in ECMP for SiC [148, 223]. The typical experimental devices are displayed in figures 19(a) and (b) and figure 20(a). According to the findings of Murata *et al* the process of SiC wafer ECMP involves electrochemically oxidizing SiC and subsequently mechanically eliminating the resulting oxide using abrasives [75], as depicted in figure 19(c). The introduction of anodic oxidation to inert SiC has led to an enhancement in MRR. In addition, Deng *et al* employed CeO<sub>2</sub> slurry as both the electrolyte for anodizing and the polishing medium for removing the oxide layer [214]. Anodization resulted in a decrease in surface hardness from 34.5 GPa to 1.9 GPa, in accordance with figure 20(b). Surface images of the diamond-abrasive-polished surface, anodically oxidized surface, and ECMP-processed surface were presented in figures 20(c)–(e), with the ECMP-treated surface exhibiting remarkable smoothness characterized by complete elimination of all scratches and RMS roughness of 0.23 nm. Compared to the CMP process, the proposed ECMP method eliminates the need for a polishing pad, thus offering a great advantage in the process cost.

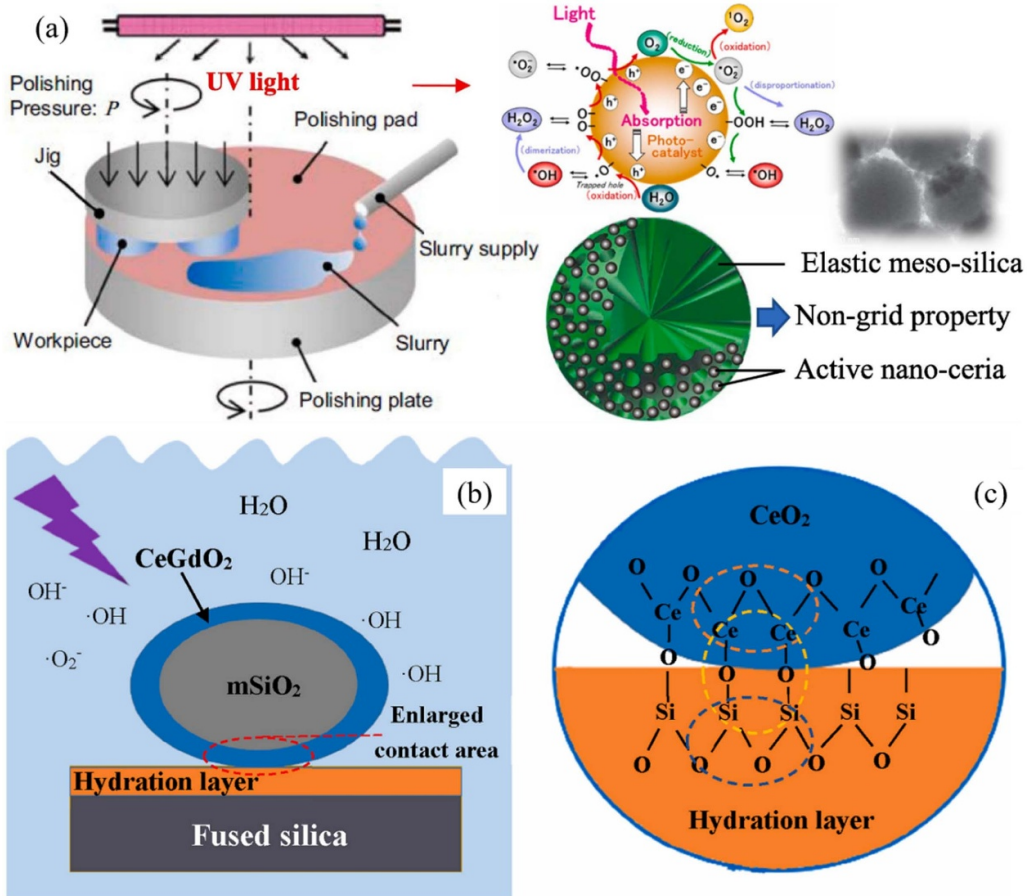


**Figure 16.** (a) Schematic images of PCMP device. (b) Interfacial contact between flexible abrasives and workpiece surfaces. (c) Tribochemical reaction between SiO<sub>2</sub> and CeO<sub>2</sub>. (a)–(c) Reprinted from [67], Copyright (2023), with permission from Elsevier.

It can be concluded that ECMP is mostly for SiC or other conductive materials or semiconductors. For FS or other glasses, such method is not applicable. The surface roughness of the ECMP surface is also not desirable since the main purpose of the method is to increase the MRR. Future studies must be conducted for the possibility of achieving lower roughness.

#### 4.3. PECMP

The occurrence of excessive oxidation on the SiC surface poses challenges in CMP/ECMP processes, leading to the presence of residual oxide layers and protrusions after polishing. Consequently, these protrusions made up of oxides can easily cause new scratches when they come into contact with abrasives, further deteriorating the smoothness of the polished surface. Moreover, the existing damages on the surface are exacerbated due to their inclination towards oxidation. In essence, achieving a flawless surface necessitates a significant reduction or elimination of both residual oxide layers and oxide protrusions present post-polishing [224]. To accomplish this objective effectively, it becomes imperative to maintain a controlled oxidation rate for the SiC surface. The environment-friendly PECMP technology has enormous potential for achieving ultra-precision SiC surfaces

due to the mild oxidation rate in photocatalytic reaction [225–227].

In SiC-PECMP, the material removal mechanisms [215] are as follows (figure 21). A novel technique for SiC-PECMP is depicted in figures 21(a) and (b), where a titanium mesh is utilized to immobilize PS/CeO<sub>2</sub> core/shell abrasives and CeO<sub>2</sub>–TiO<sub>2</sub> composite photocatalysts. When exposed to UV-light, electrons ( $e^-$ ) from the valence band (VB) of CeO<sub>2</sub> and TiO<sub>2</sub> will be excited and transferred to their respective conduction bands (CB), while simultaneously generating holes ( $h^+$ ) at their VBs according to equation (16). As shown in figure 21(c), the photogenerated  $e^-$  from the CeO<sub>2</sub> CB will migrate towards the TiO<sub>2</sub> CB due to its more positive potential compared to that of CeO<sub>2</sub>. Simultaneously, the photogenerated  $h^+$  from the TiO<sub>2</sub> VB will move towards the CeO<sub>2</sub> VB since its potential is more negative than that of TiO<sub>2</sub> VB. In other words, the composite CeO<sub>2</sub>–TiO<sub>2</sub> allows for a more efficient separation of electron–hole pairs during photocatalysis. When anodic bias is applied (figure 21(d)), the majority of generated electrons in the CeO<sub>2</sub>–TiO<sub>2</sub> composite film will be directed towards the Pt cathode through the external circuit. This facilitates further separation of electron–hole pairs, enhancing photocatalytic activity and significantly increasing the quantity of generated photogenerated  $h^+$ . Photogenerated  $h^+$  can oxidize

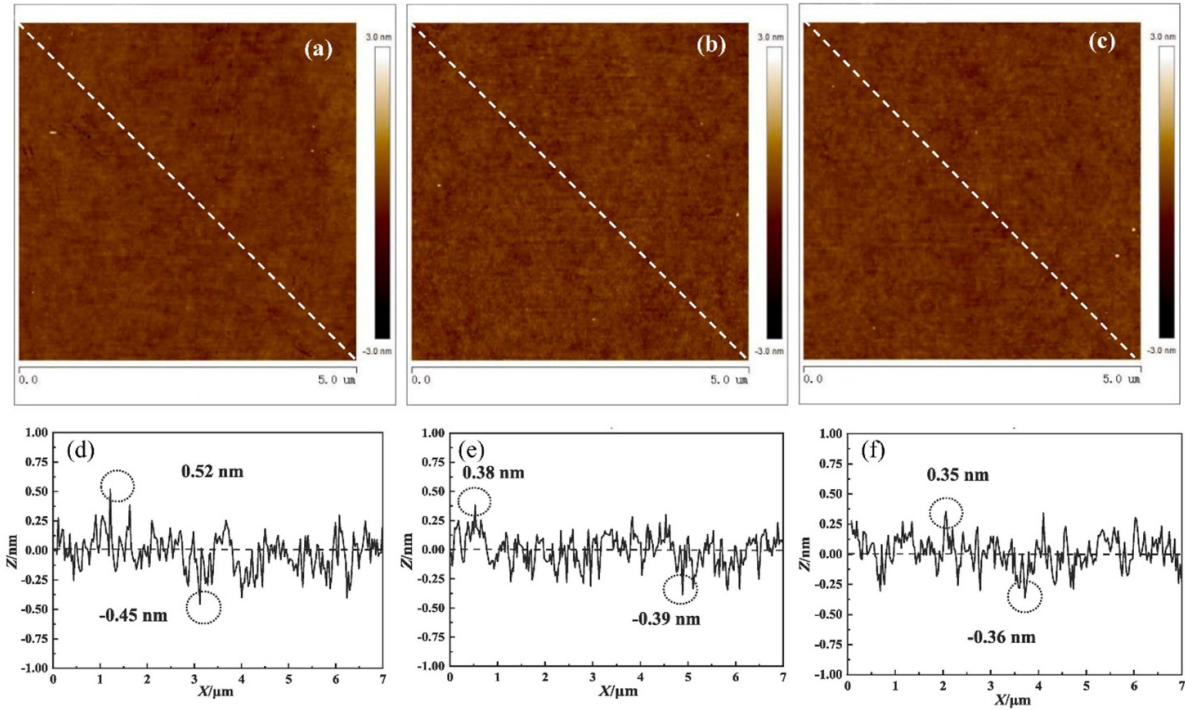


**Figure 17.** 2D-AFM images of (a) the surfaces after CMP with abrasive-A, (b) PCMP with abrasive-A, (c) PCMP with abrasive-B. Line-scan profiles of the surfaces after (d) CMP with abrasive-A, (e) PCMP with abrasive-A, and (f) PCMP with abrasive-B. (a)–(f): Reprinted from [69], Copyright (2021), with permission from Elsevier.

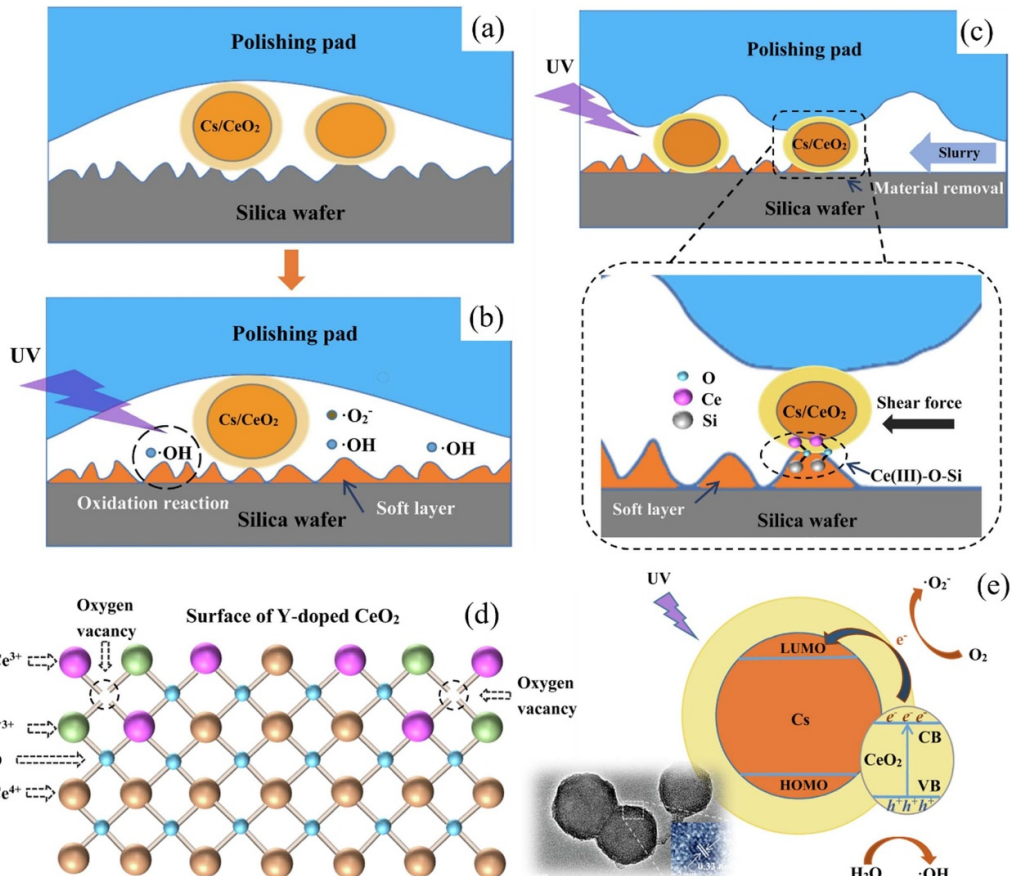


**Figure 18.** Schematics of (a) the interfacial contact, (b) the surface modification, (c) the material removal during CMP/PCMP processes using CS/CeO<sub>2</sub> functional abrasives. (d) The atomic structure of Y-doped CeO<sub>2</sub> surfaces. (e) The photooxidation mechanism toward the proposed hybrids. (a)–(e) Reprinted from [68], Copyright (2022), with permission from Elsevier.

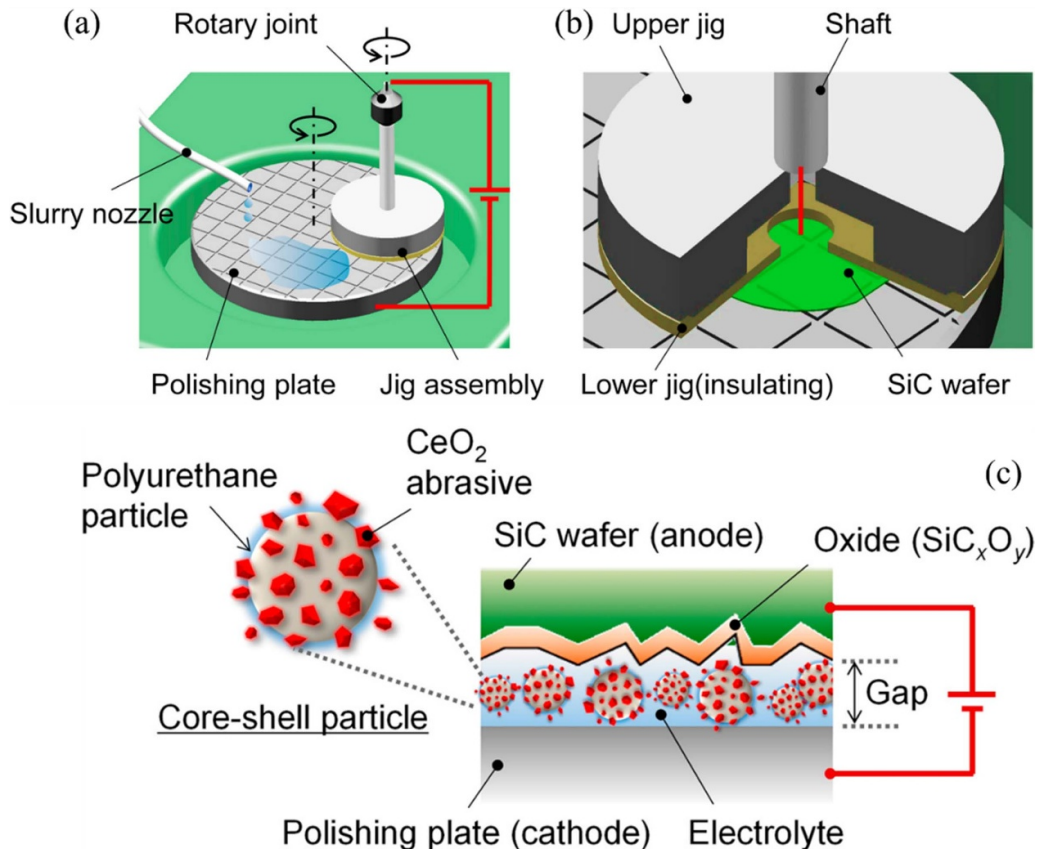


**Figure 19.** Schematic images of (a) overall, (b) cross-sectional views of the ECMP device, and (c) the ECMP mechanism. (a)–(c) Reprinted from [75], Copyright (2017), with permission from Elsevier.

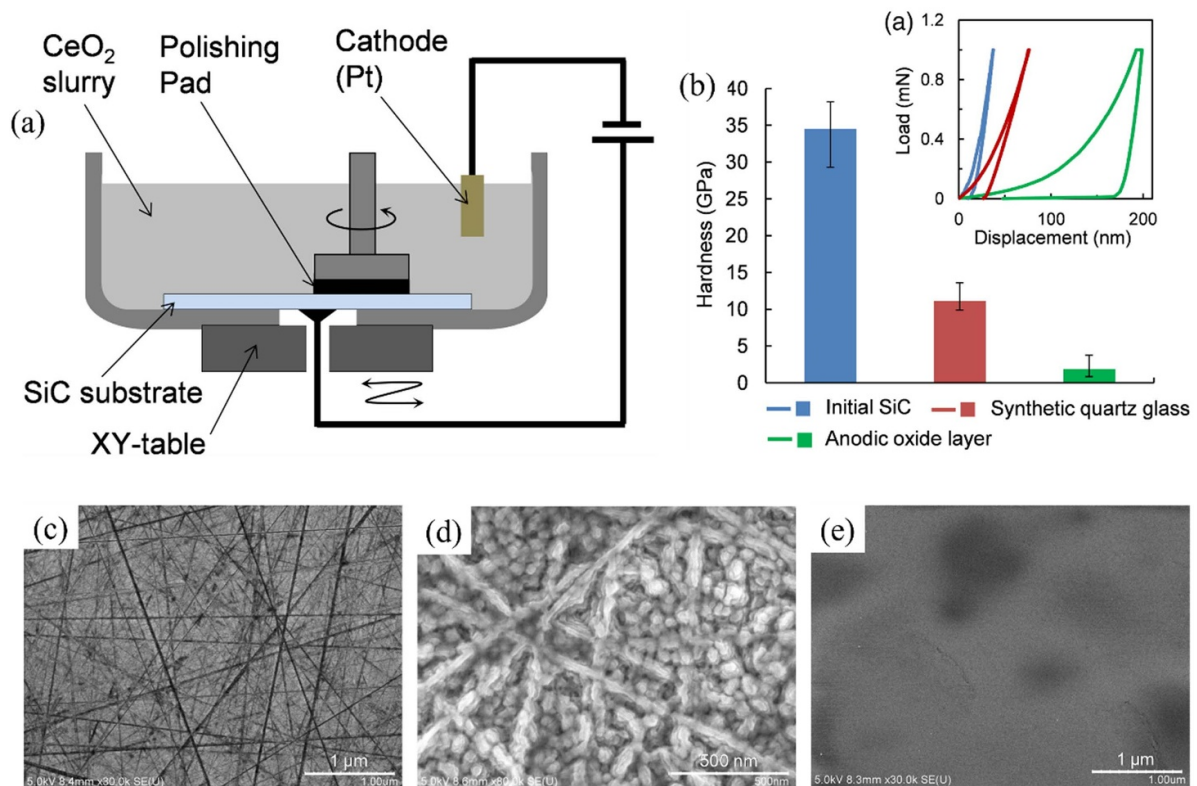


**Figure 20.** (a) Schematic images of ECMP experimental device. (b) Load-displacement curves and the hardness. SEM images of SiC surfaces after (c) diamond-abrasive-polished sample, (d) anodically oxidized sample, (e) ECMP-processed sample. (a)–(e) Reprinted from [214], Copyright (2015), with permission from Elsevier.

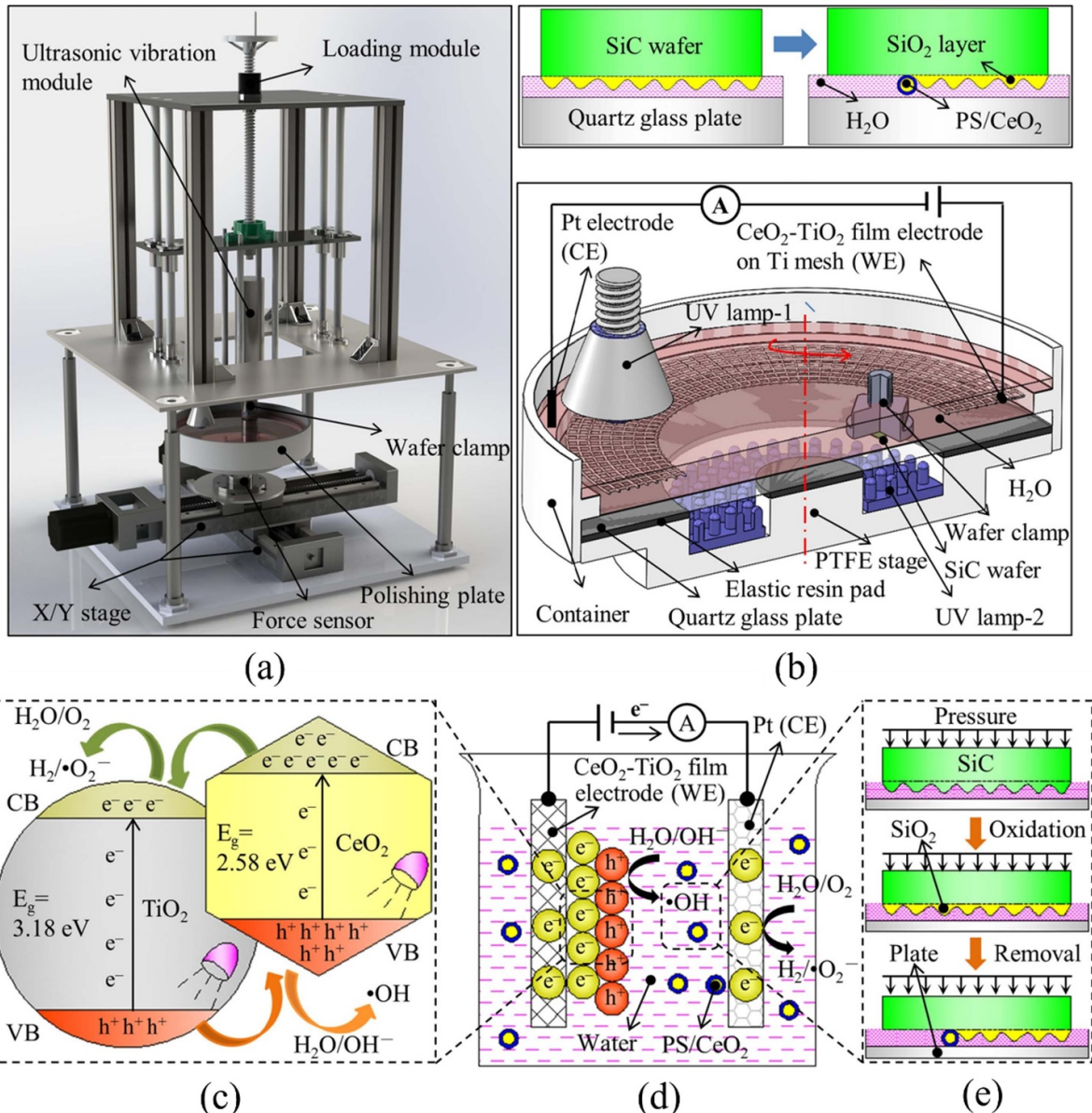
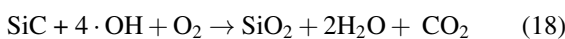


**Figure 21.** Schematic images of (a) PECMP device, (b) material removal process in SiC-PECMP. Mechanism of improving photocatalytic activity (c) by using a hetero structured CeO<sub>2</sub>-TiO<sub>2</sub> composite-film electrode, (d) by applying an anodic bias, and (e) material removal mechanisms in SiC-PECMP. (a)–(e) Reprinted from [215], Copyright (2021), with permission from Elsevier.

H<sub>2</sub>O into •OH (equation (17)), which subsequently oxidizes the SiC surface to form a soft SiO<sub>2</sub> layer (equation (18)). The PS/CeO<sub>2</sub> core/shell abrasives easily and gently remove this oxide layer, completely eliminating any surface damage with material removal (figure 21(e)),



Despite the further improvement in SiC polishing efficiency through combined assistance from electric fields and ultraviolet light, the contribution of the combined effects and

coupling effects of these two energy fields remains unknown, requiring further exploration on our part.

#### 4.4. PAP

The PAP, a novel surface treatment technique that combines atmospheric pressure water vapor plasma irradiation with abrasive polishing [228–230]. The principle of PAP technology [231] is illustrated in figure 22(a). Material removal occurs primarily through two mechanisms, as shown in figure 22(b). One involves plasma oxidation and HF immersion, while the other utilizes cerium oxide abrasive within PAP. Experimental findings indicated the presence of a thin corrosion-resistant silicon oxycarbide layer at the interface

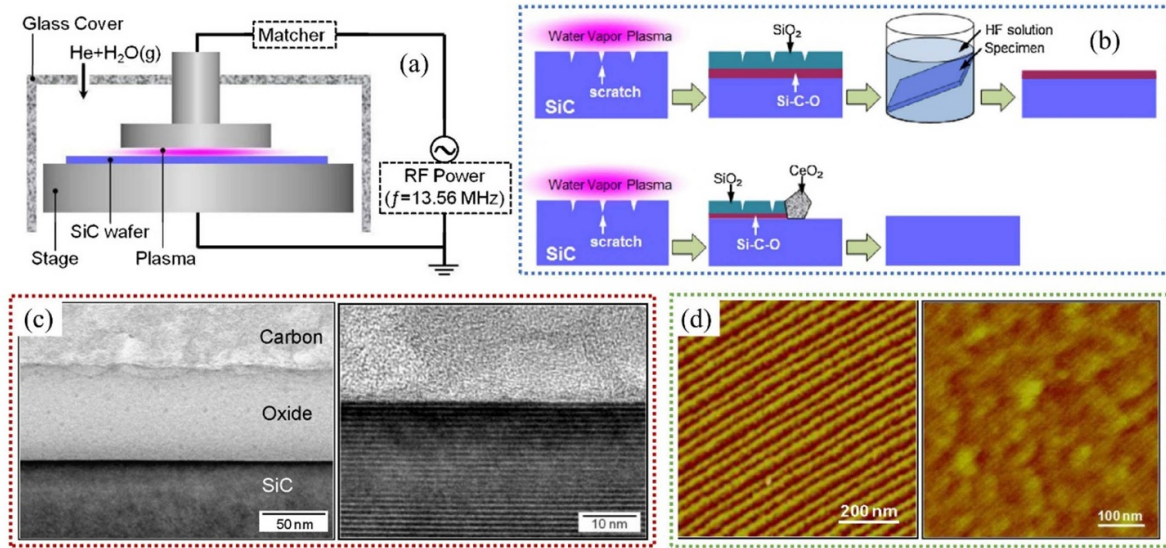


**Figure 22.** (a) Schematic images of PAP device. (b) Probable mechanism of scratch removal. (c) The XTEM and (d) AFM images of the 4 H-SiC surface before and after PAP treatment. (a)–(d) Reprinted from [231], Copyright (2013), with permission from Elsevier.

after employing the second method. The atomic plane of 4 H-SiC was achieved through a combination of steam plasma oxidation and the mechanical removal using a mild abrasive. Ultimately, this process yielded a well-ordered step/terrace morphology on the surface (figures 22(c) and (d)), devoid of any residual SiC, the surface of 4 H-SiC was successfully prepared with an RMS roughness of 0.1 nm.

## 5. Conclusion and perspectives

With the advancement of precision optics, semiconductor technology, microelectronics, and other related fields, there is a growing demand for ultra-precision atomic surfaces. Over the past decade, extensive research has been conducted on polishing media and techniques utilizing rare earth abrasives, leading to significant advancements. This paper gives a comprehensive review of the recent progress of CMP based on rare earth cerium oxide in the last two decades, including the development of new rare earth abrasives, the development of pastes, and advanced composite polishing processes for different typical materials. It can be seen from the above analysis that the surface roughness is approaching the atomic scale throughout the past decades. However, most of these works are done on small samples which can only be seen as a verification of the mechanism. And there is still a long way towards industrial application and large area atomic flatness.

In the future, the requirement of surface flatness and roughness will continue to lower, since the manufacturing accuracy and chip yield depend highly on it. Sub-2 nm chips will demand an atomic roughness, and the ultimate goal will be a surface with all atoms at the same elevation, without

any excess or absent. Rare earth abrasives have an absolute advantage in polishing silicon-containing materials due to the formation of chemical bonds during the polishing process with materials like silicon and quartz, which, through chemical mechanical action, can achieve atomic-level surface processing. However, because rare earth abrasives are softer compared to other commonly used abrasives like  $\text{Al}_2\text{O}_3$  and  $\text{SiO}_2$ , they are generally not suitable for polishing metals, metal oxides, and composite materials, which are non-silicon-based. Additionally, while rare earth composite abrasives and core-shell abrasives are effective, they are difficult to produce and expensive, further limiting the widespread application of rare earth abrasives in CMP. Therefore, future efforts should focus on simplifying the synthesis steps of rare earth abrasives, reducing synthesis costs, and producing rare earth abrasives with strong universality.

It is difficult to control the scratch depth of abrasives on the material surface uniformly in traditional CMP. To achieve an ideal smooth surface, additional physical fields must be incorporated to effectively lower the material removal volume per scratch to atomic scale. For example, laser-assisted or ultrasonic vibration-assisted polishing has been proven effective in reducing surface roughness and improving the MRR. However, since planar polishing involves securing the material between the polishing pad and the platen, integrating these energy fields into the polishing process poses a challenge for the design and development of polishing equipment. If the surface modification can be controlled to the atomic scale, while the material removal process be achieved by controllable load like nanometric vibration instead of abrasive movements, an atomic roughness can be achieved. In terms of lowering the material removal depth for each abrasive to slowly achieve the atomic roughness, the concept of removing a single layer of

atoms has been proven by previous works. In the atomic and close to atomic scale manufacturing field, it was revealed that the material removal mechanism transforms from cutting to ploughing and to pushing when the cutting depth approaches the atomic scale. But in a latest study, an atomic scale cutting phenomenon which captures the atoms after immediate elastic recovery state and achieve a cutting action at the scale of three to four atoms deep. Such phenomena shows that there are still a lot of unknown mechanism at the atomic scale for achieving atomic roughness.

## Data availability statement

All data that support the findings of this study are included within the article (and any supplementary files).

## Acknowledgment

The authors acknowledge the financial support from the National Key R&D Program of China (2018YFA0703400), the Young Scientists Fund of the National Natural Science Foundation of China (52205447), and the Changjiang Scholars Program of Chinese Ministry of Education.

## ORCID iDs

Xiangyan Chen  <https://orcid.org/0009-0001-2052-1298>  
Zhenyu Zhang  <https://orcid.org/0000-0002-2393-520X>

## References

- [1] Hossain M K, Hossain S, Ahmed M H, Khan M I, Haque N and Raihan G A 2021 A review on optical applications, prospects, and challenges of rare-earth oxides *ACS Appl. Electron. Mater.* **3** 3715–46
- [2] Luo X, Zhang Y, Zhou H, He K, Luo C, Liu Z and Tang X 2022 Review on the development and utilization of ionic rare earth ore *Minerals* **12** 554
- [3] Liu P, Bae S, Hong S, Bae C, Seo H, Lee J, Tang C and Kim T 2022 Investigation of thermal effects in copper chemical mechanical polishing *Precis. Eng.* **73** 195–202
- [4] Mei Y, Chen W and Chen X 2023 Synthesis, characterization, and polishing properties of a lanthanum cerium fluoride abrasive *Materials* **16** 3393
- [5] Kim K, Yi D K and Paik U 2017 Increase in Ce<sup>3+</sup> concentration of ceria nanoparticles for high removal rate of SiO<sub>2</sub> in chemical mechanical planarization *ECS J. Solid State Sci.* **6** 681–5
- [6] Ponader C W and Brown G E 1989 Rare earth elements in silicate glassmelt systems: II. Interactions of La, Gd, and Yb with halogens *Geochim. Cosmochim. Acta* **53** 2905–14
- [7] Kim D H, Lee E and Pak C 2021 Effect of rare-earth elements in Pd ternary alloy catalysts on activity toward oxygen reduction reaction *Catal. Today* **359** 106–11
- [8] Li H, Wang P, Lin G and Huang J 2021 The role of rare earth elements in biodegradable metals: a review *Acta Biomater.* **129** 33–42
- [9] Yuan J, Lyu B, Hang W and Deng Q 2017 Review on the progress of ultra-precision machining technologies *Front. Mech. Eng.* **12** 158–80
- [10] Wu Z, Shen J, Peng Y and Wu X 2022 Review on ultra-precision bonnet polishing technology *Int. J. Adv. Manuf. Tech.* **121** 2901–21
- [11] Hatifi S and Abou-El-Hossein K 2020 Review of single-point diamond turning process in terms of ultra-precision optical surface roughness *Int. J. Adv. Manuf. Tech.* **106** 2167–87
- [12] Guo D and Kang R 2023 State-of-the-art and perspectives of ultra-precision grinding technology for semiconductor substrates *J. Mech. Eng.* **59** 299–329
- [13] Ginsburg G S and Phillips K A 2018 Precision medicine: from science to value *Health Aff.* **37** 694–701
- [14] Zhu M and Wu Y 2023 Accuracy assessment of inertial navigation computation without initial attitude alignment *2023 DGON Inertial Sensors and Systems (ISS)* pp 1–16
- [15] He C, Zhang J, Geng K, Wang S, Luo M, Zhang X and Ren C 2022 Advances in ultra-precision machining of bearing rolling elements *Int. J. Adv. Manuf. Tech.* **122** 3493–524
- [16] Larrañaga-Altuna M *et al* 2021 Bactericidal surfaces: an emerging 21st-century ultra-precision manufacturing and materials puzzle *Appl. Phys. Rev.* **8** 021303
- [17] Wu K, Caridi A T, Gentile R J, Powell J L and Keleher J J 2022 Development of responsive polymeric nanocomposites for enhanced CeO<sub>2</sub> removal in post-chemical mechanical planarization (p-CMP) *Electrochemical Society Meeting Abstracts* pp MA2022–022353
- [18] Qiu M, Li Y, Chen L and Bai Y 2013 Effects of rare earth treatment on tribological properties of self-lubricating spherical plain bearings *Wear* **305** 274–9
- [19] Xu N, Luo Y, Lin Y, Ma J and Pu Y 2024 The influence of CeO<sub>2</sub> abrasive size on the performance of photocatalytic assisted chemical-mechanical polishing by Y/Pr co-doping strategy *Colloids Surf.* **684** 133107
- [20] Evans D R 2004 Cerium oxide abrasives—observations and analysis *MRS Proc.* **816** K9.1
- [21] Liu L, Zhang Z, Shi C, Deng X, Zhou H, Feng J, Liu X, Liu X and Wen W 2024 Angstrom surface with high material removal rate for quartz glass induced by silk dissolved novel green chemical mechanical polishing *Colloids Surf.* **682** 132957
- [22] Paik S, Kim G, Chang S, Lee S and Jin D 2020 Near-field sub-diffraction photolithography with an elastomeric photomask *Nat. Commun.* **11** 805
- [23] Zheng L, Zywiertz U, Birr T, Duderstadt M, Overmeyer L, Roth B and Reinhardt C 2021 UV-LED projection photolithography for high-resolution functional photonic components *Microsyst. Nanoeng.* **7** 64
- [24] Yang D, Shi Y and Yu X 2024 Photomask and photoresist *Handbook of Integrated Circuit Industry* (Springer) pp 1717–42
- [25] Páramo A R, Sordo F, Garoz D, Garrec B L, Perlado J M and Rivera A 2014 Transmission final lenses in the HiPER laser fusion power plant: system design for temperature control *Nucl. Fusion* **54** 123019
- [26] Betti R and Hurricane O A 2016 Inertial-confinement fusion with lasers *Nat. Phys.* **12** 435–48
- [27] Garoz D, González-Arrabal R, Juárez R, Álvarez J, Sanz J, Perlado J M and Rivera A 2013 Silica final lens performance in laser fusion facilities: hiPER and LIFE *Nucl. Fusion* **53** 013010
- [28] Armani D K, Kippenberg T J, Spillane S M and Vahala K J 2003 Ultra-high-Q toroid microcavity on a chip *Nature* **421** 925–8
- [29] Paik E Y, Zhang L, Hou S, Zhao H, Chou Y-H, Forrest S R and Deng H 2023 High quality factor microcavity for van der waals semiconductor polaritons using a transferrable mirror *Adv. Opt. Mater.* **11** 2201440
- [30] Ma N, Jiang P, Kuang N, Li S and Xu X 2023 Photonic-plasmonic hybrid microcavity with ultra-high

- quality factor regulated by bowtie plasmonic nanoantenna *Laser Optoelectron. Prog.* **60** 1525002
- [31] Li M and Xie J 2022 Green-chemical-jump-thickening polishing for silicon carbide *Ceram. Int.* **48** 1107–24
- [32] Gao B, Zhai W J, Zhai Q and Zhang M Z 2019 Novel polystyrene/CeO<sub>2</sub>-TiO<sub>2</sub> multicomponent core/shell abrasives for high-efficiency and high-quality photocatalytic-assisted chemical mechanical polishing of reaction-bonded silicon carbide *Appl. Surf. Sci.* **484** 534–41
- [33] Rusdi S, Chafidz Mas Sahid A, Nurkhamidah S, Fardhyanti D S, Handayani P A and Prasetyawan H 2022 Producing ceria (CeO<sub>2</sub>) nanoparticles using ethanol/water mixture as solvent: effect of temperature on the morphology and crystallite size *Mater. Sci. Forum* **1067** 131–7
- [34] Meng F, Zhang Z, Gao P, Liu T, Boyjoo Y and Guo D 2020 Design of composite abrasives and substrate materials for chemical mechanical polishing applications *Appl. Nanosci.* **10** 1379–93
- [35] Kalantzis P, Teugels L and De Gendt S 2017 Effect of Al<sub>2</sub>O<sub>3</sub> and SiO<sub>2</sub> abrasives on the CMP of molybdenum using different polishing parameters *ICPT 2017; Int. Conf. on Planarization/CMP Technology* pp 1–6
- [36] Chen G, Luo H, Kang C, Luo G, Zhou Y and Pan G 2019 Application of surface analysis in study on removal mechanism and abrasive selection during fused silica chemical mechanical polishing *Surf. Interface Anal.* **51** 576–83
- [37] Su J, Liu H, Qi W, Cao X and Wang Z 2020 Selection of abrasive for chemical mechanical polishing of the 304 stainless steel *J. Phys.: Conf. Ser.* **1681** 012011
- [38] Xu Y, Zhao G, Wang Q, Zhan Y and Chen B 2023 Study on material removal mechanism of sapphire wafer with CeO<sub>2</sub> coated diamond composite abrasives via green polishing *J. Manuf. Process.* **92** 412–21
- [39] Feng K, Lyu B, Zhao T, Yin T and Zhou Z 2022 Fabrication and application of gel-forming CeO<sub>2</sub> fixed abrasive tools for quartz glass polishing *Int. J. Precis. Eng. Man.* **23** 985–1002
- [40] Tsai M S 2004 Powder synthesis of nano grade cerium oxide via homogenous precipitation and its polishing performance *Mater. Sci. Eng.* **110** 132–4
- [41] Wang Z, Wang T, Zhang L and Lu X 2023 Synthesis of CeO<sub>2</sub> nanoparticles derived by urea condensation for chemical mechanical polishing *Electron. Mater. Lett.* **19** 580–7
- [42] Kim N Y, Kim G, Sun H, Hwang U, Kim J, Kwak D, Park I K, Kim T, Suhr J and Nam J D 2022 A nanoclustered ceria abrasives with low crystallinity and high Ce<sup>3+</sup>/Ce<sup>4+</sup> ratio for scratch reduction and high oxide removal rates in the chemical mechanical planarization *J. Mater. Sci.* **57** 12318–28
- [43] Ho C, Yu J C, Kwong T, Mak A C and Lai S 2005 Morphology-controllable synthesis of mesoporous CeO<sub>2</sub> nano- and microstructures *Chem. Mater.* **17** 4514–22
- [44] Oh M H, Nho J S, Cho S B, Lee J S and Singh R K 2011 Polishing behaviors of ceria abrasives on silicon dioxide and silicon nitride CMP *Powder Technol.* **206** 239–45
- [45] Lim D S, Ahn J W, Park H S and Shin J H 2005 The effect of CeO<sub>2</sub> abrasive size on dishing and step height reduction of silicon oxide film in STI-CMP *Surf. Coat. Technol.* **200** 1751–4
- [46] Yang J C, Oh D W, Lee G W, Song C L and Kim T 2010 Step height removal mechanism of chemical mechanical planarization (CMP) for sub-nano-surface finish *Wear* **268** 505–10
- [47] Wu Z, Zhang Z, Jia Y, Teng F, Li G, Wang F and Jin Y 2022 Fused silica with sub-angstrom roughness and minimal surface defects polished by ultrafine nano-CeO<sub>2</sub> *J. Am. Chem. Soc.* **106** 1766–77
- [48] Chen A, Wang S, Pan J, Wang T and Chen Y 2022 Development of Zr- and Gd-doped porous ceria (pCeO<sub>2</sub>) abrasives for achieving high-quality and high-efficiency oxide chemical mechanical polishing *Ceram. Int.* **48** 14039–49
- [49] Xu N, Ma J, Liu Q, Luo Y and Pu Y 2023 Preparation of CeO<sub>2</sub> abrasives by reducing atmosphere-assisted molten salt method for enhancing their chemical mechanical polishing performance on SiO<sub>2</sub> substrates *J. Rare Earths* **41** 1627–35
- [50] Ma J, Xu N, Luo Y, Lin Y and Pu Y 2022 Enhancing the polishing efficiency of CeO<sub>2</sub> abrasives on the SiO<sub>2</sub> substrates by improving the Ce<sup>3+</sup> concentration on their surface *ACS Appl. Electron. Mater.* **5** 526–36
- [51] Yun S S and Park J G 2020 Impact of wet ceria abrasive size on initial step height removal efficiency for Isolated SiO<sub>2</sub> film chemical mechanical planarization *J. Korean Phys. Soc.* **78** 51–57
- [52] Xu N, Ma J, Liu Q, Han W and Shan Z 2021 Size effect of CeO<sub>2</sub> particle on nanoscale single-asperity sliding friction *Tribol. Lett.* **70** 4
- [53] Liu Z, Zhang Z, Feng J, Yi X, Shi C, Gu Y, Zhao F, Liu S and Li J 2024 A novel atomic removal model for chemical mechanical polishing using developed mesoporous shell/core abrasives based on molecular dynamics *Nanoscale* **16** 85–96
- [54] He H, Wu X, Ren W, Shi P, Yao X and Song Z 2012 Synthesis of crystalline cerium dioxide hydrosol by a sol-gel method *Ceram. Int.* **38** S501–4
- [55] Hamdy A S 2006 Advanced nano-particles anti-corrosion ceria based sol gel coatings for aluminum alloys *Mater. Lett.* **60** 2633–7
- [56] Zhang L, Liu G Y, Zhu L M, Zhou T F, Guo P and Liu P 2021 Experimental study on near-polished ultra-precision grinding of fused glass with the assistant of pure CeO<sub>2</sub> atomizing liquid *Int. J. Adv. Manuf. Tech.* **115** 3243–9
- [57] Babu S V, Lee S-H, Lu Z and Matijević E 2002 Chemical mechanical polishing of thermal oxide films using silica particles coated with ceria *J. Mater. Res.* **17** 2744–9
- [58] Chen Y, Mu Z, Wang W and Chen A 2020 Development of mesoporous SiO<sub>2</sub>/CeO<sub>2</sub> core/shell nanoparticles with tunable structures for non-damage and efficient polishing *Ceram. Int.* **46** 4670–8
- [59] Kim E, Lee J, Bae C, Seok H, Kim H U and Kim T 2022 Effects of trivalent 1205 lanthanide (La and Nd) doped ceria abrasives on chemical mechanical polishing *Powder Technol.* **397** 117025
- [60] Sreeremya T S, Prabhakaran M and Ghosh S 2015 Tailoring the surface properties of cerium oxide nanoabrasives through morphology control for glass CMP *RSC Adv.* **5** 84056–65
- [61] Hu P, Chen Y, Sun R, Chen Y, Yin Y and Wang Z 2017 Synthesis, characterization and frictional wear behavior of ceria hybrid architectures with {111} exposure planes *Appl. Surf. Sci.* **401** 100–5
- [62] Lee Y, Seo Y J, Lee H and Jeong H 2016 Effect of diluted colloidal silica slurry mixed with ceria abrasives on CMP characteristic *Int. J. Precis. Eng. Man.-GT* **3** 13–17
- [63] He Q 2018 Experimental study on polishing performance of CeO<sub>2</sub> and nano-SiO<sub>2</sub> mixed abrasive *Appl. Nanosci.* **8** 163–71
- [64] Chen A, Wang T, Chen Y, Wang S and Chen Y 2022 Development of polystyrene/polyaniline/ceria (PS/PANI/CeO<sub>2</sub>) multi-component abrasives for photochemical mechanical polishing/planarization applications *Appl. Surf. Sci.* **575** 151784

- [65] Chen Y, Li Z and Miao N 2015 Polymethylmethacrylate (PMMA)/CeO<sub>2</sub> hybrid particles for enhanced chemical mechanical polishing performance *Tribol. Int.* **82** 211–7
- [66] Wang M, Mu Z, Wang T, Chen Y and Chen A 2023 Double-layered core-shell heterostructures of mSiO<sub>2</sub>@CdS@CeO<sub>2</sub> abrasive systems toward photochemical mechanical polishing (PCMP) applications *Appl. Surf. Sci.* **614** 156274
- [67] Chen Y, Zhong L, Chen A, Fu M and Lu X 2023 Highly dispersed Gd-CeO<sub>2</sub> nanocrystals supported on mesoporous silica composite particles towards photochemical (photo-assisted chemical) mechanical polishing *Ceram. Int.* **49** 16932–43
- [68] Wang T, Chen Y, Chen A and Chen Y 2022 Development of carbon sphere/ceria (CS/CeO<sub>2</sub>) heterostructured particles and their applications to functional abrasives toward photochemical mechanical polishing *Appl. Surf. Sci.* **593** 153449
- [69] Chen A, Duan Y, Mu Z, Cai W and Chen Y 2021 Meso-silica/Erbium-doped ceria binary particles as functionalized abrasives for photochemical mechanical polishing (PCMP) *Appl. Surf. Sci.* **550** 149353
- [70] Wang W, Chen Y, Chen A and Ma X 2020 Composite particles with dendritic mesoporous-silica cores and nano-sized CeO<sub>2</sub> shells and their application to abrasives in chemical mechanical polishing *Mater. Chem. Phys.* **240** 122279
- [71] Ma J, Xu N, Hu J, Luo Y, Lin Y and Pu Y 2023 Doping strategy on properties and chemical mechanical polishing performance of CeO<sub>2</sub> Abrasives: A DFT assisted experimental study *Appl. Surf. Sci.* **623** 156997
- [72] Ni Z, Chen G, Xu L, Zhang P, Dai M, Qian S, Bian D and Zhang H 2021 Preparation of ceria-coated silica nanoparticles and their chemical mechanical planarization performance on Si-Face 6H-SiC substrates *ECS J. Solid State Sci.* **10** 123011
- [73] Li Z, Jin L, Cao Z, Zhang C, Cao X, Han G, Peng S and Liu Y 2023 Development and characterization of a novel RE<sup>3+</sup> doped Core-shell CeO<sub>2</sub> abrasive system and its glass CMP investigations *Appl. Surf. Sci.* **638** 158055
- [74] Zhou C, Xu X, Dai L, Gong H and Lin S 2021 Chemical-mechanical polishing performance of core-shell structured polystyrene@ceria/nanodiamond ternary abrasives on sapphire wafer *Ceram. Int.* **47** 31691–701
- [75] Murata J, Yodogawa K and Ban K 2017 Polishing-pad-free electrochemical mechanical polishing of single-crystalline SiC surfaces using polyurethane-CeO<sub>2</sub> core-shell particles *Int. J. Mach. Tools Manuf.* **114** 1–7
- [76] Murata J, Ueno Y, Yodogawa K and Sugiura T 2016 Polymer/CeO<sub>2</sub>-Fe<sub>3</sub>O<sub>4</sub> multicomponent core-shell particles for high-efficiency magnetic-field-assisted polishing processes *Int. J. Mach. Tools Manuf.* **101** 28–34
- [77] Kim S D, Hwang I S, Park H M, Rhee J K and Nam C W 2002 Chemical mechanical polishing of shallow trench isolation using the ceria-based high selectivity slurry for sub-0.18 μm complementary metal-oxide-semiconductor fabrication *J. Vac. Sci. Technol. B* **20** 918–23
- [78] Kim S K, Yoon P W, Paik U, Katoh T and Park J G 2004 Influence of physical characteristics of ceria particles on polishing rate of chemical mechanical planarization for shallow trench isolation *Jpn. J. Appl. Phys.* **43** 7427
- [79] Lei H, Chu F, Xiao B, Tu X, Xu H and Qiu H 2010 Preparation of silica/ceria nano composite abrasive and its CMP behavior on hard disk substrate *Microelectron. Eng.* **87** 1747–50
- [80] Ryuzaki D, Hoshi Y, Machii Y, Koyama N, Sakurai H and Ashizawa T 2012 Chemical mechanical polishing with nanocolloidal ceria slurry for low-damage planarization of dielectric films *Jpn. J. Appl. Phys.* **51** 036502
- [81] Kim J S, Kang H G, Kanemoto M, Paik U and Park J G 2007 Effects of calcination and milling process conditions for ceria slurry on shallow-trench-isolation chemical-mechanical polishing performance *Jpn. J. Appl. Phys.* **46** 7671
- [82] Peedikakkandy L, Kalita L, Kayle P, Kadam A, Gujar V, Arcot M and Bhargava P 2015 Preparation of spherical ceria coated silica nanoparticle abrasives for CMP application *Appl. Surf. Sci.* **357** 1306–12
- [83] Song X, Jiang N, Li Y, Xu D and Qiu G 2008 Synthesis of CeO<sub>2</sub>-coated SiO<sub>2</sub> nanoparticle and dispersion stability of its suspension *Mater. Chem. Phys.* **110** 128–35
- [84] Sabia R and Stevens H J 2000 Performance characterization of cerium oxide abrasives for chemical-mechanical polishing of glass *Mach. Sci. Technol.* **4** 235–51
- [85] Paier J, Penschke C and Sauer J 2013 Oxygen defects and surface chemistry of ceria: quantum chemical studies compared to experiment *Chem. Rev.* **113** 3949–85
- [86] Schmitt R, Nenning A, Kraynis O, Korobko R, Frenkel A I, Lubomirsky I, Haile S M and Rupp J L M 2020 A review of defect structure and chemistry in ceria and its solid solutions *Chem. Soc. Rev.* **49** 554–92
- [87] Myong K K, Byun J, Choo M J, Kim H, Kim J Y, Lim T and Kim J J 2021 Direct and quantitative study of ceria-SiO<sub>2</sub> interaction depending on Ce<sup>3+</sup> concentration for chemical mechanical planarization (CMP) cleaning *Mater. Sci. Semicond. Process.* **122** 105500
- [88] Seo J, Gowda A and Babu S V 2018 Almost complete removal of ceria particles down to 10 nm size from silicon dioxide surfaces *ECS J. Solid State Sci.* **7** 243
- [89] Cheng J, Huang S, Li Y, Wang T, Xie L and Lu X 2020 RE (La, Nd and Yb) doped CeO<sub>2</sub> abrasive particles for chemical mechanical polishing of dielectric materials: experimental and computational analysis *Appl. Surf. Sci.* **506** 144668
- [90] Fu M, Wei L, Li Y, Zhou X, Hao S and Li Y 2009 Surface charge tuning of ceria particles by titanium doping: towards significantly improved polishing performance *Solid State Sci.* **11** 2133–7
- [91] Yuan X, Chen C, Lei H and Zhang Z 2023 Synthesis, characterization of CeO<sub>2</sub>@ZIF-8 composite abrasives and their chemical mechanical polishing behavior on glass substrate *Ceram. Int.* **49** 5189–98
- [92] Sugimoto T, Suda S and Kawahara K 2017 Change in slurry/glass interfacial resistance by chemical mechanical polishing *MRS Adv.* **2** 2205–10
- [93] Lee D, Lee H and Jeong H 2016 Slurry components in metal chemical mechanical planarization (CMP) process: a review *Int. J. Precis. Eng. Manuf.* **17** 1751–62
- [94] Liu L, Zhang Z, Wu B, Hu W, Meng F and Li Y 2021 A review: green chemical mechanical polishing for metals and brittle wafers *J. Appl. Phys.* **54** 373001
- [95] Seo J and Paik U 2016 Preparation and characterization of slurry for chemical mechanical planarization (CMP) *Advances in Chemical Mechanical Planarization (CMP)* pp 273–98
- [96] Keswani M and Han Z 2015 Post-CMP cleaning *Developments in Surface Contamination and Cleaning* ch 4, pp 145–83
- [97] Li W, Tan B, Zhang S, Gao B, Ma B, Guo L, Du H, Wang F and Wang X 2023 Application of an optimized alkaline cleaning solution for inhibitor removal during the post-CMP process: performance evaluation and mechanism analysis *J. Mol. Liq.* **369** 120892
- [98] Xu G, Zhang Z, Meng F, Liu L, Liu D, Shi C, Cui X, Wang J and Wen W 2023 Atomic-scale surface of fused silica induced by chemical mechanical polishing with controlled

- size spherical ceria abrasives *J. Manuf. Process.* **85** 783–92
- [99] Liu J, Zhang Z, Shi C, Ren Z, Feng J, Zhou H, Liu Z, Meng F and Zhao S 2023 Novel green chemical mechanical polishing of fused silica through designing synergistic CeO<sub>2</sub>/h-BN abrasives with lubricity *Appl. Surf. Sci.* **637** 157978
- [100] Zhao Z, Zhang Z, Shi C, Feng J, Zhuang X, Li L, Meng F, Li H, Xue Z and Liu D 2023 Dispersion and polishing mechanism of a novel CeO<sub>2</sub>-LaOF-based chemical mechanical polishing slurry for quartz glass *Materials* **16** 1148
- [101] Chen G, Ni Z, Xu L, Li Q and Zhao Y 2015 Performance of colloidal silica and ceria based slurries on CMP of Si-face 6H-SiC substrates *Appl. Surf. Sci.* **359** 664–8
- [102] Song X, Xu D, Zhang X, Shi X, Jiang N and Qiu G 2008 Electrochemical behavior and polishing properties of silicon wafer in alkaline slurry with abrasive CeO<sub>2</sub> *Trans. Nonferr. Metal. Soc.* **18** 178–82
- [103] Kim S K, Paik U, Oh S G, Park Y K, Katoh T and Park J G 2003 Effects of the physical characteristics of cerium oxide on plasma-enhanced tetraethylorthosilicate removal rate of chemical mechanical polishing for shallow trench isolation *Jpn. J. Appl. Phys.* **42** 1227
- [104] Cui X, Zhang Z, Shi C, Meng F, Xu G, Xie W, Liu Z, Wang J and Wen W 2022 A novel green chemical mechanical polishing for potassium dihydrogen phosphate using corn oil slurry *Mater. Today Sustain.* **20** 100257
- [105] Liu D, Zhang Z, Feng J, Yu Z, Meng F, Xu G, Wang J, Wen W and Liu W 2022 Atomic-level flatness on oxygen-free copper surface in lapping and chemical mechanical polishing *Nanoscale Adv.* **4** 4263–71
- [106] Shi N, Chen Y, Yin L, Wang Y, Zheng Z, Yan J and Han S 2023 Monodispersion of SiO<sub>2</sub>/CeO<sub>2</sub> binary nano-abrasives with adjustable size in chemical mechanical polishing performance of copper *ECS J. Solid State Sci.* **12** 074001
- [107] Yuan X, Lei H and Chen C 2024 An ethylenediaminetetraacetic acid (EDTA) surface-functionalized CeO<sub>2</sub> composite abrasives with the effective improvement of the removal rate on glass CMP *Ceram. Int.* **50** 293–305
- [108] Das D and Basu R N 2017 Organic acids as electrostatic dispersing agents to prepare high quality particulate thin film *J. Alloys Compd.* **729** 71–83
- [109] Wang Y, Zhang B, Wu P, Liu M, Cui D and Xian W 2023 Improving the dispersion stability and chemical mechanical polishing performance of CeO<sub>2</sub> slurries *ECS J. Solid State Sci.* **12** 044004
- [110] Zhang L, Xie L and Lu X 2023 Enhancing ceria slurry performance for shallow trench isolation chemical mechanical polishing through non-ionic surfactant addition *Int. J. Adv. Manuf. Tech.* **128** 4997–5010
- [111] Wei Q, Luo Z, Yang Q and Gao W 2021 Dispersion and agglomeration behaviors of submicron ceria particles in concentrated slurries *Colloid Polym. Sci.* **299** 1683–94
- [112] Abiade J T, Choi W and Singh R K 2005 Effect of pH on ceria-silica interactions during chemical mechanical polishing *J. Mater. Res.* **20** 1139–45
- [113] Wang Y, Zhang B, Wu P, Xie M, Li Y and Li H 2022 Study on preparation and polishing performance of ceria slurry 2022 *China Semiconductor Technology Int. Conf. (CSTIC)* pp 1–3
- [114] Seo Y J and Lee W S 2005 Effects of different oxidizers on the W-CMP performance *Mater. Sci. Eng.* **118** 281–4
- [115] Myong K K, Byun J, Lee J, Lim T and Kim J J 2023 Development of a pH-independent post-CMP cleaning solution using phosphoric acid-based surfactants for removal of ceria nanoparticles *ECS J. Solid State Sci.* **12** 074004
- [116] Zhu Y, Niu X, Hou Z, Zhang Y, Shi Y and Wang R 2022 Effect and mechanism of oxidant on alkaline chemical mechanical polishing of gallium nitride thin films *Mater. Sci. Semicond. Process.* **138** 106272
- [117] Zhao T, Jiang L, Liu J, Wu H, Qin N and Qian L 2021 Potassium persulfate as an effective oxidizer for chemical mechanical polishing of GCr15 bearing steel *J. Appl. Electrochem.* **51** 803–14
- [118] Xian W, Zhang B, Liu M, Wu P, Wang Y, Liu S and Cui D 2024 Optimization and mechanism of SiO<sub>2</sub>-based slurry components for atomically smooth gallium nitride surface obtained using chemical mechanical polishing technique *ECS J. Solid State Sci.* **13** 014003
- [119] Poddar M K, Jalalzai P, Sahir S, Yeriboina N P, Kim T G and Park J G 2021 Tungsten passivation layer (WO<sub>3</sub>) formation mechanisms during chemical mechanical planarization in the presence of oxidizers *Appl. Surf. Sci.* **537** 147862
- [120] Seo J 2021 A review on chemical and mechanical phenomena at the wafer interface during chemical mechanical planarization *J. Mater. Res.* **36** 235–57
- [121] Wei S, Johnson C A and Roy D 2021 Probing the mechanisms of metal CMP using tribo-electroanalytical measurements: results for a copper/malonate system *ECS J. Solid State Sci.* **10** 034001
- [122] Liu D, Zhang Z, Zhou H, Deng X, Shi C, Meng F, Yu Z and Feng J 2023 Angstrom surface on copper induced by novel green chemical mechanical polishing using ceria and silica composite abrasives *Appl. Surf. Sci.* **640** 158382
- [123] Molander G A and Cavalcanti L N 2011 Oxidation of organotrifluoroborates via Oxone *J. Org. Chem.* **76** 623–30
- [124] Alvi S, Jayant V and Ali R 2022 Applications of Oxone® in organic synthesis: an emerging green reagent of modern era *ChemistrySelect* **7** e202200704
- [125] Park S and Lee H 2021 Electrolytically ionized abrasive-free CMP (EAF-CMP) for copper *Appl. Sci.* **11** 7232
- [126] Rui X, Yongsheng W, Yipu W, Haixu L and Jianxiu S 2020 Study on oxidant in chemical mechanical polishing of copper *Trans. Electr. Electron. Mater.* **21** 580–6
- [127] Xia G, Wang Z, Yao Q, Sun P, Guan H, Wang Y, Fan C, Bian D, Zhao D and Zhao Y 2023 Modeling of material removal rate considering the chemical mechanical effects of lubricant, oxidant, and abrasive particles for aluminum chemical mechanical polishing at low pressure *Wear* **530–531** 205023
- [128] Su J X, Peng Y A, Liu Z H, Wang Z K and Fu S F 2017 Analysis on the action of oxidant in chemical mechanical polishing of 304 ultra-thin stainless steel *Mater. Sci. Forum* **893** 234–9
- [129] Lim J, Jeon B and Lee C 2001 Dry cleaning for metallic contaminants removal as the second cleaning process after the CMP process *Mater. Chem. Phys.* **70** 129–36
- [130] Dandu P R V, Peethala B C and Babu S V 2010 Role of different additives on silicon dioxide film removal rate during chemical mechanical polishing using ceria-based dispersions *J. Electrochem. Soc.* **157** H869
- [131] Park J G, Katoh T, Lee W M, Jeon H and Paik U 2003 Surfactant effect on oxide-to-nitride removal selectivity of nano-abrasive ceria slurry for chemical mechanical polishing *Jpn. J. Appl. Phys.* **42** 5420–5
- [132] Standnes D C 2021 Dissipation mechanisms for fluids and objects in relative motion described by the Navier-Stokes equation *ACS Omega* **6** 18598–609
- [133] Shin Y, Jeong J, Park Y, Jeong S, Jung H and Jeong H 2023 Modeling of step height reduction with temperature function in copper CMP *J. Mech. Sci. Technol.* **37** 6213–20

- [134] Liau L C K and Lin K 2023 Effect of slurry flow rates on tungsten removal optimization in chemical mechanical planarization *Microelectron. Reliab.* **146** 115021
- [135] Mudhavarthi S, Zantye P B, Kumar A, Kumar A, Beer bom M and Schlaf R 2005 Effect of temperature on tribological, electrochemical, and surface properties during copper CMP *Electrochem. Solid State Lett.* **8** G241
- [136] Kim N H, Seo Y J and Lee W S 2006 Temperature effects of pad conditioning process on oxide CMP: polishing pad, slurry characteristics, and surface reactions *Microelectron. Eng.* **83** 362–70
- [137] Zhang Z, Liu W and Song Z 2010 Effect of abrasive particle concentration on preliminary chemical mechanical polishing of glass substrate *Microelectron. Eng.* **87** 2168–72
- [138] Lee H, Park B and Jeong H 2009 Mechanical effect of process condition and abrasive concentration on material removal rate profile in copper chemical mechanical planarization *J. Mater. Process. Technol.* **209** 1729–35
- [139] Wang Y, Zhao Y, An W, Ni Z and Wang J 2010 Modeling effects of abrasive particle size and concentration on material removal at molecular scale in chemical mechanical polishing *Appl. Surf. Sci.* **257** 249–53
- [140] Li Y, Zhang Z, Shi C, Liu D and Liu L 2023 Density functional theory analysis and novel green chemical mechanical polishing for potassium dihydrogen phosphate *Colloids Surf.* **662** 131000
- [141] Qasim M, Parthiban P and Das D 2022 Surface planarization of CdZnTe wafers: effect of slurry formulation and CMP processing parameters on surface planarity *ECS J. Solid State Sci.* **11** 084008
- [142] Kwak D, Oh S, Kim J, Yun J and Kim T 2021 Study on the effect of ceria concentration on the silicon oxide removal rate in chemical mechanical planarization *Colloids Surf.* **610** 125670
- [143] Li G, Xiao C, Zhang S, Luo S, Chen Y and Wu Y 2023 Study of the humidity-controlled CeO<sub>2</sub> fixed-abrasive chemical mechanical polishing of a single crystal silicon wafer *Tribol. Int.* **178** 108087
- [144] Yan M, Tan B, Zhang S, Li W, Ji J, Liu Z, Huang L, Wang F, Wang X and Du H 2023 Effect of complexing agent on ceria particle removal in post-STI CMP cleaning process *Colloids Surf.* **658** 130668
- [145] Lee J, Kim E, Bae C, Seok H, Cho J, Aydin K and Kim T 2023 Improvement of oxide chemical mechanical polishing performance by increasing Ce<sup>3+</sup>/Ce<sup>4+</sup> ratio in ceria slurry via hydrogen reduction *Mater. Sci. Semicond. Process.* **159** 107349
- [146] Wu Z, Li G, Jia Y, Lv Q, Deng S and Jin Y 2023 Investigation on morphology and chemistry of the Beilby layer on polished fused silica *Ceram. Int.* **49** 17116–22
- [147] Fan Y, Jiao J, Zhao L and Tang J 2023 Preparation of lanthanide-doped polystyrene/CeO<sub>2</sub> abrasives and investigation of slurry stability and photochemical mechanical polishing performance *Colloids Surf.* **656** 130508
- [148] Murata J, Hayama K and Takizawa M 2023 Environment-friendly electrochemical mechanical polishing using solid polymer electrolyte/CeO<sub>2</sub> composite pad for highly efficient finishing of 4H-SiC (0001) surface *Appl. Surf. Sci.* **625** 157190
- [149] Deng H, Liu N, Endo K and Yamamura K 2018 Atomic-scale finishing of carbon face of single crystal SiC by combination of thermal oxidation pretreatment and slurry polishing *Appl. Surf. Sci.* **434** 40–48
- [150] Guo X, Yuan S, Huang J, Chen C-F, Kang R, Jin Z and Guo D 2020 Effects of pressure and slurry on removal mechanism during the chemical mechanical polishing of quartz glass using ReaxFF MD *Appl. Surf. Sci.* **505** 144610
- [151] Zhao F, Zhang Z, Deng X, Feng J, Zhou H, Liu Z, Meng F and Shi C 2024 Atomic surface achieved through a novel cross-scale model from macroscale to nanoscale *Nanoscale* **16** 2318–36
- [152] Netzband C M and Dunn K 2020 Controlling the cerium oxidation state during silicon oxide CMP to improve material removal rate and roughness *ECS J. Solid State Sci.* **9** 044001
- [153] Wang W, Zhang B, Shi Y, Zhou J, Wang R and Zeng N 2022 Improved chemical mechanical polishing performance in 4H-SiC substrate by combining novel mixed abrasive slurry and photocatalytic effect *Appl. Surf. Sci.* **575** 151676
- [154] Xie W, Zhang Z, Wang L, Cui X, Yu S, Su H and Wang S 2023 Chemical mechanical polishing of silicon wafers using developed uniformly dispersed colloidal silica in slurry *J. Manuf. Process.* **90** 196–203
- [155] Zhang Z, Liu J, Hu W, Zhang L, Xie W and Liao L 2021 Chemical mechanical polishing for sapphire wafers using a developed slurry *J. Manuf. Process.* **62** 762–71
- [156] Zhou Y, Huang Y, Li J, Lv W and Zhu F 2024 Investigation of the chemical action mechanism based on reactive force field in SiC chemical-mechanical polishing process *Appl. Surf. Sci.* **646** 158927
- [157] Van Bui P, Toh D, Isohashi A, Matsuyama S, Inagaki K, Sano Y, Yamauchi K and Morikawa Y 2018 Platinum-catalyzed hydrolysis etching of SiC in water: a density functional theory study *Jpn. J. Appl. Phys.* **57** 055703
- [158] Onodera T, Takahashi H and Nomura S 2020 First-principles molecular dynamics investigation of ceria/silica sliding interface toward functional materials design for chemical mechanical polishing process *Appl. Surf. Sci.* **530** 147259
- [159] Chang P, Huang Z, Ling H, Wu Y, Li M and Hang T 2024 First-principles insight into the pH-dependency of the corrosion inhibition ability of benzotriazole and 1,2,4-triazole for copper in chemical mechanical polishing slurry *Corros. Sci.* **232** 112002
- [160] Xiang C *et al* 2021 Laser soliton microcombs heterogeneously integrated on silicon *Science* **373** 99–103
- [161] Zhang L, Zheng Z and Lou X 2021 A review of WBG and Si devices hybrid applications *Chin. J. Electr. Eng.* **7** 1–20
- [162] Suzdaltsev A 2022 Silicon electrodeposition for microelectronics and distributed energy: a mini-review *Electrochim* **3** 760–8
- [163] Cui X, Zhang Z, Yu S, Chen X, Shi C, Zhou H, Meng F, Yu J and Wen W 2023 Unprecedented atomic surface of silicon induced by environmentally friendly chemical mechanical polishing *Nanoscale* **15** 9304–14
- [164] Xie L, Cheng J, Wang T and Lu X 2021 Mechanical wear behavior between CeO<sub>2</sub>(100), CeO<sub>2</sub>(110), CeO<sub>2</sub>(111), and silicon studied through atomic force microscopy *Tribol. Int.* **153** 106616
- [165] Brugnoli L, Miyatani K, Akaji M, Urata S and Pedone A 2023 New atomistic insights on the chemical mechanical polishing of silica glass with ceria nanoparticles *Langmuir* **39** 5527–41
- [166] Kotz F, Quick A S, Risch P, Martin T, Hoose T, Thiel M, Helmer D and Rapp B E 2021 Two-photon polymerization of nanocomposites for the fabrication of transparent fused silica glass microstructures *Adv. Mater.* **33** 2006341
- [167] Toombs J T, Luitz M, Cook C C, Jenne S, Li C C, Rapp B E, Kotz-Helmer F and Taylor H K 2022 Volumetric additive manufacturing of silica glass with microscale computed axial lithography *Science* **376** 308–12

- [168] Cheng J, Yang Z, Wang C, Zhao L, Chen M, Wang J, Li Y, Xu Q, Liu Z and Xu H 2022 Effect of scratches on the damage characteristics of fused silica optics under extremely-high impact load *Int. J. Mech. Sci.* **219** 107099
- [169] Guo J, Shi X, Song C, Niu L, Cui H, Guo X, Tong Z, Yu N, Jin Z and Kang R 2021 Theoretical and experimental investigation of chemical mechanical polishing of W-Ni-Fe alloy *Int. J. Extreme Manuf.* **3** 025103
- [170] Shi X, Chen G, Xu L, Kang C, Luo G, Luo H, Zhou Y, Dargusch M S and Pan G 2020 Achieving ultralow surface roughness and high material removal rate in fused silica via a novel acid SiO<sub>2</sub> slurry and its chemical-mechanical polishing mechanism *Appl. Surf. Sci.* **500** 144041
- [171] Rajendran A, Takahashi Y, Koyama M, Kubo M and Miyamoto A 2005 Tight-binding quantum chemical molecular dynamics simulation of mechano-chemical reactions during chemical-mechanical polishing process of SiO<sub>2</sub> surface by CeO<sub>2</sub> particle *Appl. Surf. Sci.* **244** 34–38
- [172] Wang L, Ren G, Xie W, Zhang J, Pan D and Wang S 2024 Simple and facile synthesis of single-crystal CeO<sub>2</sub> abrasives and its highly efficient removal mechanism on SiO<sub>2</sub> film *Appl. Surf. Sci.* **654** 159510
- [173] Shao Q, Duan S, Fu L, Lyu B, Zhao P and Yuan J 2021 Shear thickening polishing of quartz glass *Micromachines* **12** 956
- [174] Chen Y, Yeung A W K, Pow E H N and Tsui J K H 2021 Current status and research trends of lithium disilicate in dentistry: a bibliometric analysis *J. Prosthet. Dent.* **126** 512–22
- [175] Yamockul S and Thamrongananskul N 2022 Cerium oxide polishes lithium disilicate glass ceramic via a chemical-mechanical process *Eur. J. Dent.* **17** 720–6
- [176] Chen G, Li J, Long J, Luo H, Zhou Y, Xie X and Pan G 2021 Surface modulation to enhance chemical mechanical polishing performance of sliced silicon carbide Si-face *Appl. Surf. Sci.* **536** 147963
- [177] Luo Q, Lu J, Tian Z and Jiang F 2021 Controllable material removal behavior of 6H-SiC wafer in nanoscale polishing *Appl. Surf. Sci.* **562** 150219
- [178] Meng X, Wu W, Liao B and Dai H 2022 Atomic simulation of textured silicon carbide surface ultra-precision polishing *Ceram. Int.* **48** 17034–45
- [179] Ma G, Li S, Liu F, Zhang C, Jia Z and Yin X 2022 A review on precision polishing technology of single-crystal SiC *Crystals* **12** 101
- [180] Zeng Q and Sun S 2023 Recent advances in chemical mechanical polishing technologies of silicon carbide *Fine Chem. Eng.* **4** 271–87
- [181] Wang W, Lu X, Wu X, Zhang Y, Wang R, Yang D and Pi X 2023 Chemical-mechanical polishing of 4H silicon carbide wafers *Adv. Mater. Interfaces* **10** 2202369
- [182] Chen G, Pan L, Luo H, Zhou Y, Luo G and Pan G 2023 Chemical mechanical polishing of silicon carbide (SiC) based on coupling effect of ultrasonic vibration and catalysis *J. Environ. Chem. Eng.* **11** 111080
- [183] Deng H, Endo K and Yamamura K 2015 Competition between surface modification and abrasive polishing: a method of controlling the surface atomic structure of 4H-SiC (0001) *Sci. Rep.* **5** 8947
- [184] Yin X, Li S and Chai P 2020 Investigation of SiC single crystal polishing by combination of anodic oxidation and mechanical polishing *Int. J. Electrochem. Sci.* **15** 4388–405
- [185] Carter P W and Johns T P 2005 Interfacial reactivity between ceria and silicon dioxide and silicon nitride surfaces *Electrochem. Solid State Lett.* **8** G218
- [186] Mariscal J C, McAllister J, Sampurno Y, Suarez J S, O'Neill M, Zhou H, Grief M, Slutz D and Philipossian A 2020 Tribological, thermal and kinetic characterization of SiO<sub>2</sub> and Si<sub>3</sub>N<sub>4</sub> polishing for STI CMP on blanket and patterned wafers *ECS J. Solid State Sci.* **9** 044008
- [187] Wortman-Otto K M, Linhart A N, Dudek A L, Sherry B M and Keleher J J 2021 Role of molecular structure on modulating the interfacial dynamics for shallow trench isolation (STI) chemical mechanical planarization (CMP) applications *ECS J. Solid State Sci.* **10** 024009
- [188] Park T, Kim T, Son C and Lim S 2023 Passivation of poly-Si surface using vinyl and epoxy group additives for selective Si<sub>3</sub>N<sub>4</sub> etching in H<sub>3</sub>PO<sub>4</sub> solution *Appl. Surf. Sci.* **608** 155143
- [189] Lee S P, Tseng T H, Chuang C H, Chuang C Y, Cheng C H, Tung H Y, Huang P C and Chou C T 2019 Chemical-mechanical polishing (CMP) process of STI and DTI- Ching-Yu Hsieh 2019 *Joint Int. Symp. on e-Manufacturing & Design Collaboration(eMDC) & Semiconductor Manufacturing (ISSM)* pp 1–4
- [190] Nomura S, Lee S, Yanagisawa M and Homma T 2021 Observation of polymer additive absorption on substrates for STI CMP slurries *ECS Meet. Abstr.* **MA2021-01** 819
- [191] Herfurth N, Adesunkanni A A, Zwicker G and Boit C 2023 Reliable backside IC preparation down to STI level using chemical mechanical polishing (CMP) with highly selective slurry *Int. Symp. for Testing and Failure Analysis (ISTFA)* pp 265–70
- [192] Bae K, Baek K H, Kim J, Kim H, Yoon B U and Kim J J 2017 Highly selective chemical mechanical polishing of Si<sub>3</sub>N<sub>4</sub> over SiO<sub>2</sub> using advanced silica abrasive *Jpn. J. Appl. Phys.* **56** 056501
- [193] Jiang M, Wood N O and Komanduri R 1998 On chemo-mechanical polishing (CMP) of silicon nitride (Si<sub>3</sub>N<sub>4</sub>) workmaterial with various abrasives *Wear* **220** 59–71
- [194] Wang Z, Pang M, Liang M, Yao J G, Lijie M and Su J 2020 The effect of slurries on lapping performance of fixed abrasive pad for Si<sub>3</sub>N<sub>4</sub> ceramics *Sci. Prog.* **103** 0036850420982451
- [195] Zhang L, Xie L and Lu X 2023 Effect of ionic surfactants in ceria-based slurries on shallow trench isolation chemical mechanical polishing *SSRN Electronic Journal*
- [196] Wortman-Otto K M, Saucedo C and Keleher J J 2019 Role of additive structure on controlling ceria/substrate interactions relevant to shallow trench isolation (STI) chemical mechanical planarization (CMP) *ECS Meet. Abstr.* **MA2019-01** 2161
- [197] Kang H G, Paik U, Park H S and Park J G 2007 Effects of abrasive particle size and molecular weight of poly(acrylic acid) in ceria slurry on removal selectivity of SiO<sub>2</sub>/Si<sub>3</sub>N<sub>4</sub> films in shallow trench isolation chemical mechanical planarization *J. Mater. Res.* **22** 777–87
- [198] Oh M H, Singh R K, Gupta S and Cho S B 2010 Polishing behaviors of single crystalline ceria abrasives on silicon dioxide and silicon nitride CMP *Microelectron. Eng.* **87** 2633–7
- [199] Stetsovych O, Beran J, Dvořák F, Mašek K, Mysliveček J and Matolín V 2013 Polarity driven morphology of CeO<sub>2</sub>(100) islands on Cu(111) *Appl. Surf. Sci.* **285** 766–71
- [200] Yang X, Liang S, Wang X, Xiao P and Fan Z 2010 Effect of WC and CeO<sub>2</sub> on microstructure and properties of W-Cu electrical contact material *Int. J. Refract. Hard Met.* **28** 305–11
- [201] Xu N, Han W, Wang Y, Li J and Shan Z 2017 Nanoscratching of copper surface by CeO<sub>2</sub> *Acta Mater.* **124** 343–50
- [202] Chen A, Long J, Li Z and Chen Y 2018 Copper chemical mechanical polishing performances of polystyrene/ceria hybrid abrasives with a core/shell structure *J. Inorg. Organomet. Polym. Mater.* **28** 1655–63

- [203] Zhang T, Wang Z, Wang Y and Chen Z 2019 Experimental study on the mechanical properties of oxygen-free copper used in high energy physics detectors and accelerators *Nucl. Instrum. Methods Phys. Res. A* **935** 8–16
- [204] Wang T and Lei H 2019 Novel polyelectrolyte-Al<sub>2</sub>O<sub>3</sub>/SiO<sub>2</sub> composite nanoabrasives for improved chemical mechanical polishing (CMP) of sapphire *J. Mater. Res.* **34** 1073–82
- [205] Mei E, Liu X, Chen Y, Yu Y, Chen Z, Yang K, Liang X and Xiang W 2021 Modified  $\alpha$ -Al<sub>2</sub>O<sub>3</sub> wafer: enhance the stability of perovskite quantum dots with wide colour gamut for white light-emitting diodes *Appl. Surf. Sci.* **569** 150964
- [206] Lei H, Tong K and Wang Z 2016 Preparation of Ce-doped colloidal SiO<sub>2</sub> composite abrasives and their chemical mechanical polishing behavior on sapphire substrates *Mater. Chem. Phys.* **172** 26–31
- [207] Xu Y, Lin C, Wang Q, Zheng C, Zhan Y and Chen B 2022 A novel polishing process with rigid-flexible composite structure plate for sapphire wafer polishing *Int. J. Adv. Manuf. Tech.* **122** 659–68
- [208] Zhou M, Cheng Y, Zhong M and Xu W 2023 Macro and micro-nano machining mechanism for ultrasonic vibration assisted chemical mechanical polishing of sapphire *Appl. Surf. Sci.* **640** 158343
- [209] Li Z, Deng Z and Hu Y 2020 Effects of polishing parameters on surface quality in sapphire double-sided CMP *Ceram. Int.* **46** 13356–64
- [210] Kou Z, Wang C, Zhou W, Chen A and Chen Y 2024 Trivalent lanthanum and ytterbium doped meso-silica/ceria abrasive systems toward chemical mechanical polishing (CMP) and ultraviolet irradiation-assisted photochemical mechanical polishing (PCMP) *Appl. Surf. Sci.* **657** 159733
- [211] Xu N, Luo Y, Ma J, Lin Y, Zhu X and Pu Y 2024 Enhancement mechanism of Y-doped Ce<sub>1-x</sub>Y<sub>x</sub>O<sub>2</sub> for photocatalytic-assisted chemical-mechanical polishing *Mater. Today Commun.* **38** 107791
- [212] Inada N, Takizawa M, Adachi M and Murata J 2024 Sustainable Electrochemical Mechanical Polishing (ECMP) for 4H-SiC wafer using chemical-free polishing slurry with hydrocarbon-based solid polymer electrolyte *Appl. Surf. Sci.* **664** 160241
- [213] Murata J and Nagatomo D 2020 Investigation of electrolytic condition on abrasive-free electrochemical mechanical polishing of 4H-SiC using Ce thin film *ECS J. Solid State Sci.* **9** 034002
- [214] Deng H, Hosoya K, Imanishi Y, Endo K and Yamamura K 2015 Electro-chemical mechanical polishing of single-crystal SiC using CeO<sub>2</sub> slurry *Electrochim. Commun.* **52** 5–8
- [215] Gao B, Zhai W, Zhai Q and Wang C 2021 Novel photoelectrochemically combined mechanical polishing technology for scratch-free 4H-SiC surface by using CeO<sub>2</sub>-TiO<sub>2</sub> composite photocatalysts and PS/CeO<sub>2</sub> core/shell abrasives *Appl. Surf. Sci.* **570** 151141
- [216] Ma W, Mashimo T, Tamura S, Tokuda M, Yoda S, Tsushima M, Koinuma M, Kubota A, Isobe H and Yoshiasa A 2020 Cerium oxide (CeO<sub>2-x</sub>) nanoparticles with high Ce<sup>3+</sup> proportion synthesized by pulsed plasma in liquid *Ceram. Int.* **46** 26502–10
- [217] Yamamura K, Tatsuya T, Masaki U, Azusa N H and Nobuyuki Z 2010 High-integrity finishing of 4H-SiC (0001) by plasma-assisted polishing *Adv. Mater. Res.* **126–128** 423–42
- [218] Deng H, Takiguchi T, Ueda M, Hattori A N, Zettsu N and Yamamura K 2011 Damage-free dry polishing of 4H-SiC combined with atmospheric-pressure water vapor plasma oxidation *Jpn. J. Appl. Phys.* **50** 08JG05
- [219] Deng H, Ueda M and Yamamura K 2014 Characterization of 4H-SiC (0001) surface processed by plasma-assisted polishing *Int. J. Adv. Manuf. Tech.* **72** 1–7
- [220] Deng H, Endo K and Yamamura K 2014 Polishing characteristics of single crystal SiC assisted by plasma oxidation using different kinds of abrasives *Proc. 14th Euspen Int. Conf.*
- [221] Yan Q, Wang X, Xiong Q, Lu J and Liao B 2020 The influences of technological parameters on the ultraviolet photocatalytic reaction rate and photocatalysis-assisted polishing effect for SiC *J. Cryst. Growth* **531** 125379
- [222] Yu X, Zhang B, Wang R, Kao Z, Yang S and Wei W 2021 Effect of photocatalysts on electrochemical properties and chemical mechanical polishing rate of GaN *Mater. Sci. Semicond. Process.* **121** 105387
- [223] Gao B, Zhai W J, Zhai Q and Shi Y Q 2020 Polystyrene/CeO<sub>2</sub> core-shell abrasives for high-quality 4H-SiC surface in ECMP: the effects of shell thickness *ECS J. Solid State Sci.* **9** 044005
- [224] Yang X, Yang X, Kawai K, Arima K and Yamamura K 2021 Novel SiC wafer manufacturing process employing three-step slurryless electrochemical mechanical polishing *J. Manuf. Process.* **70** 350–60
- [225] Dong Z, Ou L, Kang R, Hu H, Zhang B, Guo D and Shi K 2019 Photoelectrochemical mechanical polishing method for n-type gallium nitride *CIRP Ann.* **68** 205–8
- [226] Qiao L, Ou L and Shi K 2023 Wireless photoelectrochemical mechanical polishing for inert compound semiconductor wafers *J. Manuf. Process.* **88** 97–109
- [227] Ou L, Wang Y, Hu H, Zhang L, Dong Z, Kang R, Guo D and Shi K 2019 Photochemically combined mechanical polishing of N-type gallium nitride wafer in high efficiency *Precis. Eng.* **55** 14–21
- [228] Yamamura K, Takiguchi T, Ueda M, Deng H, Hattori A N and Zettsu N 2011 Plasma assisted polishing of single crystal SiC for obtaining atomically flat strain-free surface *CIRP Ann.* **60** 571–4
- [229] Lyu P, Lai M, Liu Z and Fang F 2021 Ultra-smooth finishing of single-crystal lutetium oxide by plasma-assisted etching *Precis. Eng.* **67** 77–88
- [230] Lyu P, Lai M, Liu Z and Fang F 2023 Atomic and close-to-atomic scale polishing of Lu<sub>2</sub>O<sub>3</sub> by plasma-assisted etching *Int. J. Mech. Sci.* **252** 108374
- [231] Deng H and Yamamura K 2013 Atomic-scale flattening mechanism of 4H-SiC (0001) in plasma assisted polishing *CIRP Ann.* **62** 575–8